SCIENCE AND TECHNOLOGY ORGANIZATION
CENTRE FOR MARITIME RESEARCH AND EXPERIMENTATION

Reprint Series **CMRE-PR-2019-088**

Modeling vessel kinematics using a stochastic mean-reverting process for long-term prediction

Leonardo M. Millefiori, Paolo Braca, Karna Bryan, Peter Willett

June 2019

Originally published in:

IEEE Transactions on Aerospace and Electronic Systems, volume 52, issue 5, October 2016, pp. 2313-2330, doi: 10.1109/TAES.2016.150596

About CMRE

The Centre for Maritime Research and Experimentation (CMRE) is a world-class NATO scientific research and experimentation facility located in La Spezia, Italy.

The CMRE was established by the North Atlantic Council on 1 July 2012 as part of the NATO Science & Technology Organization. The CMRE and its predecessors have served NATO for over 50 years as the SACLANT Anti-Submarine Warfare Centre, SACLANT Undersea Research Centre, NATO Undersea Research Centre (NURC) and now as part of the Science & Technology Organization.

CMRE conducts state-of-the-art scientific research and experimentation ranging from concept development to prototype demonstration in an operational environment and has produced leaders in ocean science, modelling and simulation, acoustics and other disciplines, as well as producing critical results and understanding that have been built into the operational concepts of NATO and the nations.

CMRE conducts hands-on scientific and engineering research for the direct benefit of its NATO Customers. It operates two research vessels that enable science and technology solutions to be explored and exploited at sea. The largest of these vessels, the NRV Alliance, is a global class vessel that is acoustically extremely quiet.

CMRE is a leading example of enabling nations to work more effectively and efficiently together by prioritizing national needs, focusing on research and technology challenges, both in and out of the maritime environment, through the collective Power of its world-class scientists, engineers, and specialized laboratories in collaboration with the many partners in and out of the scientific domain.

NOTE: The CMRE Reprint series reprints papers and articles published by CMRE authors in the open literature as an effort to widely disseminate CMRE products. Users are encouraged to cite the original article where possible.

Modeling Vessel Kinematics Using a Stochastic Mean-Reverting Process for Long-Term Prediction

LEONARDO M. MILLEFIORI, Member, IEEE
PAOLO BRACA, Member, IEEE
KARNA BRYAN
Centre for Maritime Research and Experimentation
La Spezia, Italy

PETER WILLETT, Fellow, IEEE
University of Connecticut, Storrs
CT, USA

We present a novel method for predicting long-term target states based on mean-reverting stochastic processes. We use the Ornstein-Uhlenbeck (OU) process, leading to a revised target state equation and to a time scaling law for the related uncertainty that in the long term is shown to be orders of magnitude lower than under the nearly constant velocity (NCV) assumption. In support of the proposed model, an analysis of a significant portion of real-world maritime traffic is provided.

Manuscript received August 26, 2015; revised February 9, 2016; released for publication May 20, 2016.

DOI. No. 10.1109/TAES.2016.150596.

Refereeing of this contribution was handled by L. Mihaylova.

Authors' addresses: L. M. Millefiori, P. Braca, K. Bryan, Centre for Maritime Research and Experimentation, Research Department, Viale San Bartolomeo 400, La Spezia, 19126 Italy; P. Willett, University of Connecticut, ECE Department, 371 Fairfield Road, U-1157, University of Connecticut, Storrs, CT 06269-9005. Corresponding author is P. Braca, E-mail: (paolo.braca@cmre.nato.int).

I. INTRODUCTION

NATO's 2011 Alliance Maritime Strategy (AMS) [2] highlights the strategic importance of the maritime environment as quoted in the following excerpt.

> The oceans connect nations globally through an interdependent network of economic, financial, social and political relationships. 70% of the Earth is covered in water; 80% of the world's population lives within 100 miles of the coast; 90% of the world's commerce is seaborne and 75% of that trade passes through a few, vulnerable, canals and international straits. The maritime environment includes trade routes, choke points, ports, and other infrastructure such as pipelines, oil and natural gas platforms, and trans-oceanic telecommunications cables.

Special emphasis is given to the maritime security environment as one of its most important operative scenarios, and surveillance is a crucial component of these activities. Ship traffic monitoring is a foundation for many maritime security domains (e.g. law enforcement, search and rescue (SaR), environmental protection, and resource management), and modern monitoring system specifications and requirements reflect the need for an extended and continuous ability to track vessels beyond territorial waters and within several sensor coverage areas. However, vessels in open seas are seldom continuously observed by monitoring sensors and even the data coming from self-reporting systems is often highly intermittent. These coverage gaps clearly represent a high risk in terms of safety at sea.

The problem of long-term vessel state estimate and prediction is therefore crucial. Unfortunately, this issue has been overlooked in the target tracking literature, and only few works partially address the problem, e.g. see [26, 27, 33], while most of the literature is focused on maneuvering target models, e.g. see [20, 28, 35]. The analysis of real-world self-reported data [i.e., largely automatic identification system (AIS)] shows that a significant portion of the vessels in open seas maneuver very seldom. In the literature, nonmaneuvering target dynamics are modeled with a velocity that is perturbed by a white noise process. This model is often referred as nearly constant velocity (NCV) [3, 28] and has been successfully used in several target tracking applications, such as radar [21] and sonar [6] where the prediction step always refers to the very near future, generally one sensor time-scan ahead. The NCV model is adopted also in [27] for anomaly detection and motion prediction.

We propose a novel method for the long-term prediction of target states based on the Ornstein-Uhlenbeck (OU) stochastic process, which leads to a revised target state equation and to a completely different time scaling law for the related uncertainty. This novel formulation reduces by orders of magnitude the uncertainty region of the predicted position with respect to the models available in literature.

This aspect is crucial for several applications. In SaR operations, a smaller uncertainty region implies a smaller search region, which can significantly improve the probability of success for search cases. For instance, let us consider a vessel having an accident in a region with intermittent AIS coverage (e.g. open sea); the position of the accident is consequently unknown. Not having any information other than its last observed position and the time of accident (e.g. time of SOS message), the only possibility is to hypothesize that the ship had been moving from the last observation to the position of the accident in a straight line. It is important to notice that this assumption has to be made whether the traditional or the proposed approach is taken; the important difference is that using the proposed method the search area (the uncertainty region) would increase linearly—instead of quadratically—in proportion to the time from last report, for a given level of confidence. In the counterpiracy framework [17], vessels can keep their AIS transmitters off for several hours when sailing in dangerous areas, in order not to be detected by pirates. The use of the proposed modeling would provide a good clue about their position even when their last broadcast message is several hours old. Also the association of synthetic aperture radar (SAR) vessel detections with AIS contacts would greatly benefit from the proposed modeling in terms of reduction of ambiguities because of the narrower gating region, especially in open sea where AIS coverage might be poor. From another standpoint, a smaller uncertainty region of the long-term prediction may reduce the probability of missing a vessel of interest in a high-resolution SAR acquisition, which has to be planned several hours ahead of the platform passing above the target.

The OU model is popular in various and heterogeneous scientific fields, spanning from physics [13, 16, 18, 31] to finance [4, 8] and biology [5, 30], but is much less popular within the tracking community [29]. The OU stochastic process was first introduced in physics [13, 18, 31] to describe the velocity of a Brownian particle under the influence of friction. It can be seen as a modified Wiener process so that there is a tendency of the walk to move back towards a central location, with a greater attraction when the process is further away from the center. OU processes have been used also in finance, e.g. [4], to model the instantaneous variance of stock price volatility, and more recently in the context of high-frequency trading [8]. In biology, the OU process has been adopted as a baseline model for animal movement [5]. In [30] the authors considered a spatial neuron model in which the membrane potential satisfies an equation with an input current, which is a dynamic random process of the OU type.

To the best of the authors' knowledge only a few authors propose the OU model for the target dynamics, and none of them address its appealing properties for long-term prediction. In the tracking literature the OU model has been discussed mostly notably by Coraluppi and Carthel in [9–12], where the stability of the OU, and

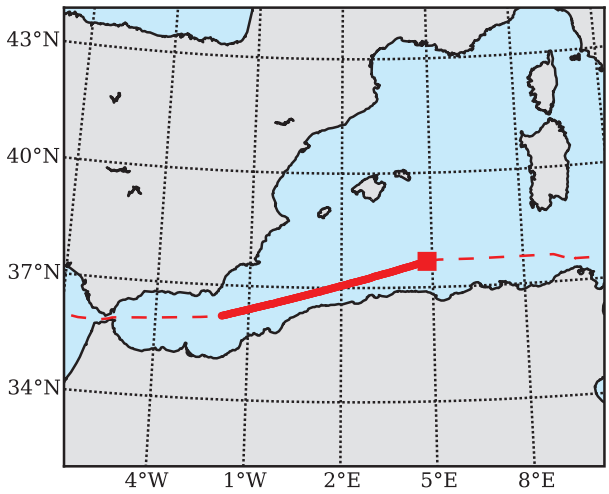

Fig. 1. Trajectory of the target under consideration: a tanker vessel of 270 meters in length and 48 in breadth sailing northeastwards from the Gibraltar Strait to the East Mediterranean. The dashed line represents the entire trajectory of the vessel, but only the highlighted portion has been considered, in order for the nonmaneuverability hypothesis to be satisfied. The red square denotes the last contact in the considered sequence.

the so-called mixed Ornstein-Uhlenbeck (MOU) processes are studied.

However all of these works, including [29], deal with zero-mean-reverting processes, i.e., the typical velocities are null, being the aim not the long-term target state prediction, but rather the short-term characterization of the target dynamics. Indeed, in [10] authors are more interested in the boundedness of the target components, and for this reason the MOU is constructed in order to be a zero-mean-reverting process for both position and velocity.[1]

Differently from [9–12, 29], in this paper we focus on the long-term prediction of nonmaneuvering vessels, such as those under way in open sea. Our thesis is that the NCV model might be implausible for a significant portion of maritime ship traffic, as vessels under way tend to continuously adjust their speeds around a desired operating point. This fundamental difference between the OU and NCV models is well explained intuitively by the case of study shown in Figs. 1 and 2, where a real-world vessel is sailing in the Mediterranean Sea with a desired speed. In the uppermost plot of Fig. 2 the actual velocity of the vessel is reported, while the lowermost plots contain one hundred realizations of the velocity using simulated OU and NCV models having the same initial point as the real trajectory. The velocity samples drawn from the OU process are bounded around the average value, as indeed are the actual velocity samples, while in the simulated

[1] In [9–12, 29], the OU is a process in which the target position follows an OU dynamic, while the integrated Ornstein-Uhlenbeck (IOU) is a process in which the target velocity follows an OU dynamic while the position is integrated. We follow a different nomenclature, used in the statistic literature [4], in which velocities are OU and then positions are IOU.

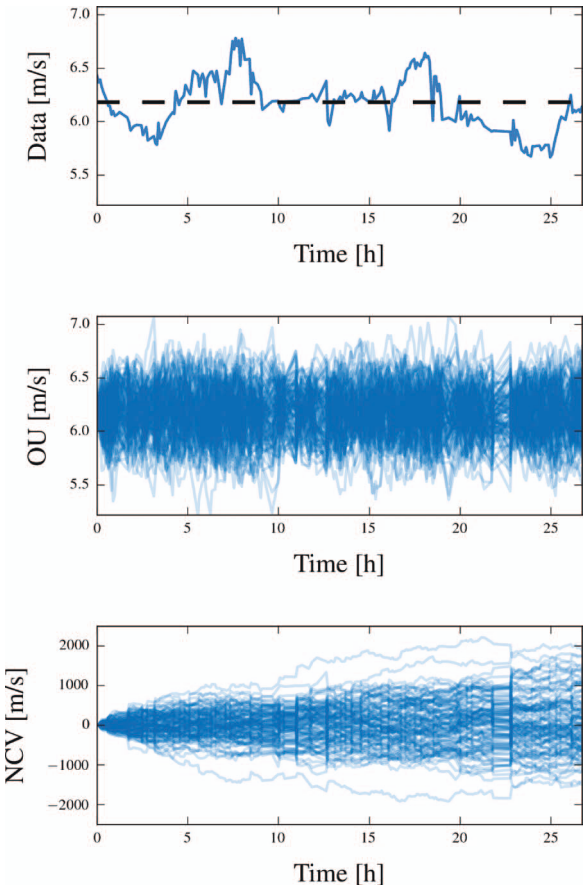

Fig. 2. Single-component velocity of the real-world vessel trajectory illustrated in Fig. 1: the uppermost plot shows the actual velocity samples; the middle plot is for a simulated OU process; the lowermost plot illustrates a simulated NCV process. Simulated processes use as initial state the first velocity sample of the real-world trajectory; the process parameters are estimated from the data series shown at the top of this figure.

NCV case the velocity apparently tends to diverge. In other words, in the long term the NCV model does not seem to be well suited for the representation of the vessel velocity.

Supported by real-world vessel traffic data, the main result presented in this work is that mean-reverting processes can be used to model nonmaneuvering vessel movement. Specifically, we provide evidence that the vessel velocity is well described by an OU stochastic process, and consequently the vessel position by an IOU process. As a consequence, after an initial transient, the vessel position is mathematically equivalent to a Brownian particle motion. It is also shown that the popular NCV model that is commonly adopted in the target tracking literature is not well suited for the characterization of the uncertainty of the long-term target state prediction. While it is sufficiently accurate for short-term predictions (meaning typically the case for traditional target tracking applications) the NCV model can overestimate the actual uncertainty of long-term predictions, even to orders of magnitude.[2]

The results are supported by an extensive analysis of a data set of real-world vessel trajectories. For each of them, the OU and NCV process parameters are estimated using a maximum likelihood (ML) procedure. The OU and NCV models are then compared in terms of capability to represent statistically the prediction error variance against the prediction horizon time. Specifically, two different ad hoc validation criteria are proposed: 1) the experimental normalized prediction variance curve, averaged among the all the available trajectories, is compared against the theoretical normalized variance curve of the OU and NCV models; 2) for each vessel trajectory, a hypothesis testing procedure is applied, this consisting of deciding, at each available time, whether or not the prediction error variance is compatible with the theoretical models, meaning significantly larger (or smaller) variance than the theoretical value. Based on both the validation criteria, the OU process models better than the NCV the behavior of a significant portion of real-world vessels. The proposed estimator, based on the OU process, is then demonstrated to be suitable for long-term prediction in practical applications. Moreover, the prediction uncertainty equation has a closed-form expression, provided by the OU process characterization, which is very useful in real-world use cases. Furthermore, in this paper we offer the closed-form expression for the solution of the coupled OU and IOU stochastic differential equation (SDE), not available in the target tracking literature.

The data set of trajectories comes from AIS [1, 23] positioning reports broadcast by vessels. The AIS is a self-reporting system originally conceived for collision avoidance. However, there are increasing possibilities for the use of AIS beyond this scope: the amount of information reported by onboard AIS transceivers is impressive, and for reference in Fig. 3 we report the density of traffic in the world computed using AIS data collected during six months at the NATO Science and Technology Organization (STO) Centre for Maritime Research and Experimentation (CMRE). AIS data is often used for scientific purposes, for instance as ground truth in order to estimate the performance of coastal radars [21].

The analysis herein presented is based on two months of commercial maritime traffic data recorded in the Mediterranean Sea during year 2014. The behavior of a vessel, and especially a nonmaneuvering one, depends greatly on its size and tonnage and consequently the motion characteristics may differ significantly among different categories. Consequently, we considered it worthwhile to subdivide the data set into three smaller ones, each of them being representative of a traffic category: cargo, tanker, and passenger vessels. Specifically, we observe, respectively, 1370 cargo, 370 tanker, and 150 passenger trajectories, collecting in total about 200 000 AIS messages.

The paper is organized as follows. In Section II we formalize the problem in terms of SDE for the target motion and introduce the OU and NCV models. Section III is devoted to the model parameter estimation procedure, while in Section IV the validation criteria of

[2] Preliminary results have been reported in [22, 25].

Fig. 3. Density of AIS messages collected from multiple AIS networks from April to September 2012. Each pixel covers a 4 nmi (one-fifteenth-degree) square on the ground and its color is (logarithmically) proportional to the number of ships whose reported positions fall within its footprint.

the prediction models are formalized. Finally, experimental results are reported in Section V and some mathematical derivations are given in the appendices.

II. VESSEL DYNAMIC MODELS

In this section we describe the stochastic models of the vessel (or target) dynamics. Let us indicate the target state at time $t \in \mathbb{R}_0^+$ with

$$\boldsymbol{s}(t) \stackrel{def}{=} [x(t),\ y(t),\ \dot{x}(t),\ \dot{y}(t)]^T, \tag{1}$$

where the two coordinates $x(t)$ and $y(t)$, and the corresponding velocities $\dot{x}(t)$ and $\dot{y}(t)$, in a two-dimensional Cartesian (x, y) reference system are also denoted by

$$\boldsymbol{x}(t) \stackrel{def}{=} [x(t),\ y(t)]^T \tag{2}$$

$$\dot{\boldsymbol{x}}(t) \stackrel{def}{=} [\dot{x}(t),\ \dot{y}(t)]^T. \tag{3}$$

The choice to define the target state in the Cartesian coordinates is standard in the target tracking literature, e.g. see [3]. In this formulation of the problem (x, y) can be either the Universal Transverse Mercator (UTM) coordinate system, or the rotated coordinate along the target trajectory as usually assumed in the knowledge-based tracking, e.g. see [7, 34, 36].

Let the target dynamics be a set of linear SDE in the form [28]:

$$\mathrm{d}\boldsymbol{s}(t) = \boldsymbol{A}\boldsymbol{s}(t)\,\mathrm{d}t + \boldsymbol{G}\boldsymbol{u}(t)\,\mathrm{d}t + \boldsymbol{B}\,\mathrm{d}\boldsymbol{w}(t), \tag{4}$$

where $\boldsymbol{A}$, $\boldsymbol{B}$, and $\boldsymbol{G}$ are constant matrices, $\boldsymbol{u}(t)$ is a deterministic function, and $\boldsymbol{w}(t)$ is a standard bidimensional Wiener process. The SDE can be solved by the use of Itô calculus [24].

Given the state of a target $\boldsymbol{s}(t_0)$ observed at the time t_0, we aim to predict its state at the time t. The prediction is carried out by the optimal Bayesian estimator:

$$\begin{aligned}\boldsymbol{s}(t|t_0) &\stackrel{def}{=} [x(t|t_0),\ y(t|t_0),\ \dot{x}(t|t_0),\ \dot{y}(t|t_0)]^T \\ &= \mathrm{E}\left[\boldsymbol{s}(t)\,|\boldsymbol{s}(t_0)\right],\end{aligned} \tag{5}$$

where $\mathrm{E}[\cdot]$ indicates the expected value operator. As opposed to conventional tracking applications, we are more interested in exploring the properties of $\boldsymbol{s}(t|t_0)$ when $t - t_0$ is not comparable to the refresh rate of the sensor that issues the measurements, being instead orders of magnitude above it. The estimator is highly dependent on the underlying motion model described by the SDE (4); in this work we focus only on the case of nonmaneuvering vessels while under way.

It is worth mentioning that in the tracking literature the target state observation is typically affected by noise. We assume to observe directly the target positional state.[3]

One of the most popular target motion models, commonly adopted in the scientific target tracking literature, is the NCV model [28], where (4) has the form

$$\mathrm{d}\boldsymbol{s}(t) = \boldsymbol{A}\boldsymbol{s}(t)\,\mathrm{d}t + \boldsymbol{B}\,\mathrm{d}\boldsymbol{w}(t), \tag{6}$$

with

$$\boldsymbol{A} = \begin{bmatrix} \mathbf{0} & \boldsymbol{I} \\ \mathbf{0} & \mathbf{0} \end{bmatrix}, \quad \boldsymbol{B} = \begin{bmatrix} \mathbf{0} \\ \boldsymbol{C} \end{bmatrix}, \tag{7}$$

being $\boldsymbol{I}$ the bidimensional identity matrix, $\mathbf{0}$ the bidimensional null matrix, and $\boldsymbol{C}$ a generic bidimensional matrix. In practice, the equation for the target dynamics relies on the fact that for nonmaneuvering vessels $\ddot{\boldsymbol{x}}(t) \approx [0, 0]^T$, i.e., there is a "small" effect on $\dot{\boldsymbol{x}}(t)$ that accounts for unpredictable modeling errors [28].

For the OU model the SDE has a slightly different form, with an additional term that accounts for the mean-reverting tendency of the velocity:

$$\mathrm{d}\boldsymbol{s}(t) = \boldsymbol{A}\boldsymbol{s}(t)\,\mathrm{d}t + \boldsymbol{G}\,\boldsymbol{v}\,\mathrm{d}t + \boldsymbol{B}\,\mathrm{d}\boldsymbol{w}(t), \tag{8}$$

where $\boldsymbol{v} = [v_x, v_y]^T$, and $\boldsymbol{w}(t)$ is a standard bidimensional Wiener process. The matrices $\boldsymbol{A}$, $\boldsymbol{B}$, and $\boldsymbol{G}$ are defined as

$$\boldsymbol{A} = \begin{bmatrix} \mathbf{0} & \boldsymbol{I} \\ \mathbf{0} & -\boldsymbol{\Theta} \end{bmatrix}, \quad \boldsymbol{B} = \begin{bmatrix} \mathbf{0} \\ \boldsymbol{C} \end{bmatrix}, \quad \boldsymbol{G} = \begin{bmatrix} \mathbf{0} \\ \boldsymbol{\Theta} \end{bmatrix}, \tag{9}$$

being $\boldsymbol{\Theta}$ and $\boldsymbol{C}$ generic bidimensional matrices. Equation (8) has the form of a Langevin dynamic [18] and can be solved in closed form by using Itô calculus [16, 24], see details in Appendix A. The $\dot{\boldsymbol{x}}(t)$ process is said to be of OU type [4, 31] and correspondingly, we say that $\boldsymbol{x}(t)$ is an IOU process [4]. The parameters v_x and v_y in $\boldsymbol{v} = [v_x, v_y]^T$ play a key role in the proposed model because they represent the typical velocities along x and y, respectively, of the vessel on the trajectory under consideration. Roughly speaking, the velocity of the process tends to drift over time towards its long-term mean; and the mean-reversion tendency is stronger when the velocity is further away from that long-term mean. In [9, 10, 29] the OU zero-mean-reverting process is introduced, in which the parameters v_x and v_y are both null. Furthermore the Singer model [28] provides for the target acceleration to be modeled as an OU zero-mean-reverting process. However, in both cases the aim is not the long-term target state prediction, but rather the short-term characterization of the target dynamics.

The diagonal terms of $\boldsymbol{\Theta}$ represent the mean reversion effect along the x and y components, respectively, while the off-the-diagonal elements are representative of the coupling effect between them. Assuming that $\boldsymbol{\Theta}$ is diagonalizable and has positive eigenvalues, an affine transformation can be found that projects the matrix $\boldsymbol{\Theta}$ onto another space, i.e., $\boldsymbol{\Theta} = \boldsymbol{R}\boldsymbol{\Gamma}\boldsymbol{R}^{-1}$, where $\boldsymbol{\Gamma}$ is diagonal. We expand this idea further in Appendix A, where we also provide the general solution to the coupled problem.

A. Prediction Procedure

The solution of the SDE provides for the target state prediction $\boldsymbol{s}(t|t_0)$ and the related variance, which we take as a measure of the prediction uncertainty. In this section we describe the prediction procedure in the two cases that the OU and NCV models are assumed for the target velocity.

1) *NCV Model*: Assuming the NCV model for the velocity of the target, we have that the optimal prediction, given the initial target state $\boldsymbol{s}(t_0)$, is the following [3]

$$\boldsymbol{s}(t|t_0) = \boldsymbol{F}(t - t_0)\boldsymbol{s}(t_0), \tag{10}$$

where $\boldsymbol{F}(t)$ is often referred to as the state transition matrix and is given by

$$\boldsymbol{F}(t) = \begin{bmatrix} \boldsymbol{I} & t\,\boldsymbol{I} \\ \mathbf{0} & \boldsymbol{I} \end{bmatrix}. \tag{11}$$

According to (10), the covariance matrix of the estimator is provided by the solution obtained by Itô calculus and is given by

$$\mathrm{Cov}\left[\boldsymbol{s}(t)\,|\boldsymbol{s}(t_0)\right] = \begin{bmatrix} \frac{(t-t_0)^3}{3} & \frac{(t-t_0)^2}{2} \\ \frac{(t-t_0)^2}{2} & t - t_0 \end{bmatrix} \otimes \boldsymbol{C}\boldsymbol{C}^T, \tag{12}$$

where

$$\boldsymbol{C}\boldsymbol{C}^T = \begin{bmatrix} \sigma_x^2 & \sigma_{xy} \\ \sigma_{xy} & \sigma_y^2 \end{bmatrix}.$$

A slightly different process noise assumption of the NCV (see [3]), would lead to the same estimator (10) but with a higher scaling law of the errors, i.e., proportional to $(t–t_0)^4/4$ instead of $(t–t_0)^3/3$ for the position and proportional to $(t–t_0)^2$ instead of $(t–t_0)$ for the velocity. In common tracking applications, where the time interval is fixed, the two models are quite similar because the parameters $\sigma_{x,y}$ can be differently tuned in order to compensate for the different scaling laws. But in the present work, even if the parameters were tuned differently, the two models would still behave differently in the long term.[4]

2) *OU Model*: Let us consider the case in which the velocity of the target follows the OU model. For the sake of clarity we assume hereafter that $\boldsymbol{\Theta} = \boldsymbol{\Gamma} = \mathrm{diag}\,(\boldsymbol{\gamma})$ is diagonal and $\boldsymbol{\gamma} = [\gamma_x, \gamma_y]^{\mathrm{T}}$. The general solution is provided in Appendix A.

[3] The assumption of the measurement noise being absent is even plausible with respect to the real-world data set presented in Section V and therein exploited for the prediction error variance analysis, because the vessel positions broadcast by AIS transmitters have the same accuracy as the Global Positioning System (GPS), and the measurement noise would be therefore negligible.

[4] It is not a trivial matter to decide whether the t^3 scale law is more suitable than the t^4 one for our purposes. In the analysis with real-world data presented in Section V, we provide results for both versions of the NCV model.

We have that the optimal prediction, given the initial target state, is provided by the first moment of the SDE solution [4, 16] and, for the velocity, we have

$$\dot{\boldsymbol{x}}(t|t_0) = \boldsymbol{v} + \begin{bmatrix} \mathrm{e}^{-\gamma_x(t-t_0)} & 0 \\ 0 & \mathrm{e}^{-\gamma_y(t-t_0)} \end{bmatrix} (\dot{\boldsymbol{x}}(t_0) - \boldsymbol{v}). \quad (13)$$

Proceeding similarly for the target position, which is an IOU process, the following expression can be derived

$$\boldsymbol{x}(t|t_0) = \boldsymbol{x}(t_0) + (t - t_0)\,\boldsymbol{v} + \begin{bmatrix} \frac{1-\mathrm{e}^{-\gamma_x(t-t_0)}}{\gamma_x} & 0 \\ 0 & \frac{1-\mathrm{e}^{-\gamma_y(t-t_0)}}{\gamma_y} \end{bmatrix} (\dot{\boldsymbol{x}}(t_0) - \boldsymbol{v}). \quad (14)$$

The optimal prediction can be rearranged in the matrix form

$$\boldsymbol{s}(t|t_0) = \boldsymbol{\Phi}(t - t_0,\ \boldsymbol{\gamma})\,\boldsymbol{s}(t_0) + \boldsymbol{\Psi}(t - t_0,\ \boldsymbol{\gamma})\,\boldsymbol{v}, \quad (15)$$

where $\boldsymbol{\Phi}(t, \boldsymbol{\gamma})$ is the analog of the state transition matrix and $\boldsymbol{\Psi}(t, \boldsymbol{\gamma})\,\boldsymbol{v}$ is often called the control input function. Their definitions are respectively provided by (46) and (48) in Appendix A.

The estimator covariance is provided in (51) in Appendix A. The variance terms are reported here:

$$\mathrm{E}\left[(x(t|t_0) - x(t))^2 |\boldsymbol{s}(t_0)\right] = \frac{\sigma_x^2}{\gamma_x^3} f(\gamma_x\,(t - t_0)) \quad (16)$$

$$\mathrm{E}\left[(y(t|t_0) - y(t))^2 |\boldsymbol{s}(t_0)\right] = \frac{\sigma_y^2}{\gamma_y^3} f\left(\gamma_y\,(t - t_0)\right) \quad (17)$$

$$E\left[(\dot{x}(t|t_0) - \dot{x}(t))^2 |\boldsymbol{s}(t_0)\right] = \frac{\sigma_x^2}{\gamma_x} g(\gamma_x\,(t - t_0)) \quad (18)$$

$$E\left[(\dot{y}(t|t_0) - \dot{y}(t))^2 |\boldsymbol{s}(t_0)\right] = \frac{\sigma_y^2}{\gamma_y} g\left(\gamma_y\,(t - t_0)\right) \quad (19)$$

where $f(t)$ and $g(t)$ are the prediction position and velocity error normalized variance, defined as

$$f(t) \stackrel{def}{=} \frac{1}{2}\left(2t + 4\mathrm{e}^{-t} - \mathrm{e}^{-2t} - 3\right) \quad (20)$$

$$g(t) \stackrel{def}{=} \frac{1}{2}\left(1 - \mathrm{e}^{-2t}\right) \quad (21)$$

being σ_x^2 and σ_y^2 the diagonal elements of $\boldsymbol{C}\boldsymbol{C}^T$.

REMARK Interestingly, it is easy to show that when $\gamma_{x,y} = 0$ the two models are equivalent because they have the same dynamic expressions. Furthermore, by applying l'Hôpital's rule to (15) when $\gamma_{x,y} \to 0$ then $\boldsymbol{\Phi}(t - t_0, \boldsymbol{\gamma}) \to \boldsymbol{F}(t - t_0)$ while $\boldsymbol{\Psi}(t - t_0, \boldsymbol{\gamma}) \to \boldsymbol{0}$, and again by applying l'Hôpital's rule the OU covariance (51) degenerates in the NCV covariance (12).

III. PARAMETER ESTIMATION PROCEDURE

In support of our thesis that the motion of a nonmaneuvering ship in open sea is better represented by an OU process on the target velocity rather than the NCV model, we present an analysis of a significant real-world data set of vessel trajectories in order to compare the SDE models described in the previous section. For this reason we need a procedure to establish the SDE parameters $\boldsymbol{\theta} = (\boldsymbol{\theta}_x, \boldsymbol{\theta}_y)$ of the processes. In the NCV case

$$\boldsymbol{\theta}_x = \sigma_x \text{ and } \boldsymbol{\theta}_y = \sigma_y \quad (22)$$

while, under the OU assumption on the target velocity, we have

$$\boldsymbol{\theta}_x = (\sigma_x, \gamma_x, v_x) \text{ and } \boldsymbol{\theta}_y = \left(\sigma_y, \gamma_y, v_y\right). \quad (23)$$

To keep the notation light, we use hereafter the notation $\boldsymbol{\theta}_{x,y}$, $\sigma_{x,y}$, $\gamma_{x,y}$, and $v_{x,y}$ to denote quantities that can equally refer to the x or y coordinate.

In this section we provide a description of the procedure that has been adopted to estimate $\boldsymbol{\theta}$ for every given trajectory. Let us assume we have recorded a set of K trajectories of nonmaneuvering vessels. In practice, the nonmaneuverability assumption translates to the selection of piecewise linear vessel trajectories. Each trajectory is defined by a set of target states

$$\mathcal{S}_i = \left\{\boldsymbol{s}_i(t_{i,j})\right\}_{j=0}^{N_i}, \quad (24)$$

for $i = 1, \ldots, K$ at some time instants $t_{i,j-1} (< t_{i,j})$, for $j = 0, \ldots, N_i$. We assume to observe only the set of velocities denoted by

$$\mathcal{Z}_i = \left\{\dot{\boldsymbol{x}}_i(t_{i,j})\right\}_{j=0}^{N_i},$$

for $i = 1, \ldots, K$. Every trajectory i is characterized by $\boldsymbol{\theta}_i = (\boldsymbol{\theta}_{x,i}, \boldsymbol{\theta}_{y,i})$, which is estimated from the measurement set $\mathcal{Z}_i$ for both the NCV and OU models. Thanks to the Markovian and Gaussian properties of (6) and (8) [24, 32], the likelihood function of $\mathcal{Z}_i$ is explicitly given by [32]

$$\mathcal{L}_i(\boldsymbol{\theta}_i) = \prod_{j=1}^{N_i} \phi\left(\dot{\boldsymbol{x}}_i(t_{i,j}) \left| \dot{\boldsymbol{x}}_i(t_{i,j-1}), \boldsymbol{\theta}_i \right.\right), \quad (25)$$

where $\phi(\cdot)$ is a bivariate Gaussian distribution. The estimate is then provided by the ML estimator

$$\hat{\boldsymbol{\theta}}_i = \arg\max_{\boldsymbol{\theta}} \mathcal{L}_i(\boldsymbol{\theta}).$$

However, in order to simplify the estimation procedure from a computational perspective, we can use the marginal likelihood along the x and y coordinates. This marginalization procedure is quite standard, especially from the Bayesian standpoint (assuming noninformative prior in our case) i.e., the other coordinate (y if we are estimating parameters along x and vice versa) is considered as a nuisance parameter. The marginal likelihoods are then given by

$$\mathcal{L}_{x,i}\left(\boldsymbol{\theta}_{x,i}\right) = \prod_{j=1}^{N_i} \phi_{\dot{x}_i}\left(\dot{x}_i(t_{i,j}) \left| \dot{x}_i(t_{i,j-1}), \boldsymbol{\theta}_{x,i} \right.\right), \quad (26)$$

$$\mathcal{L}_{y,i}\left(\boldsymbol{\theta}_{y,i}\right) = \prod_{j=1}^{N_i} \phi_{\dot{y}_i}\left(\dot{y}_i(t_{i,j}) \left| \dot{y}_i(t_{i,j-1}), \boldsymbol{\theta}_{y,i} \right.\right). \quad (27)$$

where $\phi_{\dot{x}_i}(\cdot)$ and $\phi_{\dot{y}_i}(\cdot)$ are Gaussian distributions with mean and variance given by the solution of the SDE (see

also the discussion in Section II). Specifically, for the NCV we have

$$\mathrm{E}\left[\dot{x}_i(t_{i,j})\,\middle|\,\dot{x}_i(t_{i,j-1})\right] = \dot{x}_i(t_{i,j-1}) \tag{28a}$$

$$\mathrm{E}\left[\dot{y}_i(t_{i,j})\,\middle|\,\dot{y}_i(t_{i,j-1})\right] = \dot{y}_i(t_{i,j-1}) \tag{28b}$$

$$\mathrm{V}\left[\dot{x}_i(t_{i,j})\,\middle|\,\dot{x}_i(t_{i,j-1})\right] = \sigma_x^2\Delta_{i,j} \tag{28c}$$

$$\mathrm{V}\left[\dot{y}_i(t_{i,j})\,\middle|\,\dot{y}_i(t_{i,j-1})\right] = \sigma_y^2\Delta_{i,j} \tag{28d}$$

while for the OU we have

$$\mathrm{E}\left[\dot{x}_i(t_{i,j})\,\middle|\,\dot{x}_i(t_{i,j-1})\right] = v_x + (\dot{x}_i(t_{i,j-1}) - v_x)\mathrm{e}^{-\gamma_x\Delta_{i,j}} \tag{29a}$$

$$\mathrm{E}\left[\dot{y}_i(t_{i,j})\,\middle|\,\dot{y}_i(t_{i,j-1})\right] = v_y + (\dot{y}_i(t_{i,j-1}) - v_y)\mathrm{e}^{-\gamma_y\Delta_{i,j}} \tag{29b}$$

$$\mathrm{V}\left[\dot{x}_i(t_{i,j})\,\middle|\,\dot{x}_i(t_{i,j-1})\right] = \frac{\sigma_x^2}{\gamma_x}\,g\left(\gamma_x\Delta_{i,j}\right) \tag{29c}$$

$$\mathrm{V}\left[\dot{y}_i(t_{i,j})\,\middle|\,\dot{y}_i(t_{i,j-1})\right] = \frac{\sigma_y^2}{\gamma_y}\,g\left(\gamma_y\Delta_{i,j}\right) \tag{29d}$$

where $\mathrm{V}[\cdot]$ indicates the variance operator and $\Delta_{i,j} \overset{def}{=} t_{i,j} - t_{i,j-1}$. The ML estimators along x and y for the i^{th} trajectory are given by

$$\begin{aligned}\hat{\boldsymbol{\theta}}_{x,i} &= \arg\max_{\boldsymbol{\theta}_x} \mathcal{L}_{x,i}\left(\boldsymbol{\theta}_x\right),\\ \hat{\boldsymbol{\theta}}_{y,i} &= \arg\max_{\boldsymbol{\theta}_y} \mathcal{L}_{y,i}\left(\boldsymbol{\theta}_y\right).\end{aligned} \tag{30}$$

Further details about the implementation of the ML estimators are given in Appendix B.

IV. MODEL VALIDATION CRITERIA

In this section we describe the validation methods used against the NCV and OU models, based on the capability of the model not only to predict future target states but also to quantify the uncertainty of the prediction. For this reason, the validation is carried out by analyzing the properties of the prediction error.

Let us consider the i^{th} trajectory, which is made up of a sequence of target states $\mathcal{S}_i$, as in (24), observed at the time instants $t_{i,j-1}$ ($< t_{i,j}$). For the purpose of model validation, in the prediction procedure we take each data point of the trajectory and, using it as the initial target state, we perform the target state prediction at the time instants of the following observations. That is, given the initial state $\boldsymbol{s}_i(t_{i,j})$ for $j = 0,1,\ldots,N_i$, we predict the sequence of target states at the time instants $t = t_{i,n}$ for $n = j+1,\ldots,N_i$:

$$\hat{\mathcal{S}}_i = \left\{\left\{\boldsymbol{s}_i(t_{i,n}|t_{i,j})\right\}_{n=j+1}^{N_i}\right\}_{j=0}^{N_i},$$

where the estimate $\boldsymbol{s}_i(t_{i,n}|t_{i,j})$ is given by (10) for the NCV model, and by (15) for the OU model. The parameters $\boldsymbol{\theta}_i$ used in the prediction are estimated from the velocity samples themselves, as described in Section III.

We can now define the prediction error as a function of the prediction horizon $t > 0$:

$$\begin{aligned}\boldsymbol{e}_{\boldsymbol{s}_i}(t) &\overset{def}{=} \left[\boldsymbol{e}_{\boldsymbol{x}_i}^T(t), \boldsymbol{e}_{\dot{\boldsymbol{x}}_i}^T(t)\right]^T\\ &= \boldsymbol{s}_i(t+t_0) - \boldsymbol{s}_i(t+t_0|t_0),\end{aligned} \tag{31}$$

which is a zero-mean random variable. The dependency on the generic instant t_0 is not made explicit in the notation because we are interested only in its first and second moments, which are independent of t_0 because of the properties of the target process described in Section II.

Therefore, we consider hereafter that $t_0 = 0$, without affecting the analysis. Having predicted the target states at the time instants when the measurements are available, the prediction intervals for the i^{th} trajectory are

$$\mathcal{T}_i = \left\{\left\{t_{i,n} - t_{i,j}\right\}_{n=j+1}^{N_i}\right\}_{j=1}^{N_i},$$

meaning that the prediction error is sampled at the time instants $t \in \mathcal{T}_i$. The computed prediction error should correspond to the diagonal elements of (12) in the NCV case, and to (16)–(19) under the OU assumption on the target velocity. In order to verify the suitability of the models under investigation for the prediction uncertainty, we analyze the set of prediction errors $\{\boldsymbol{e}_{\boldsymbol{s}_i}(t)\}_{i=1}^K$ for both models versus the prediction horizon t.

A. Prediction Error Variance Criterion

In this section we propose a validation criterion based on the comparison between the sample prediction error variance, as computed from the real-world data, and the theoretical variance, as expected from the SDE models.

The first hurdle is related to the fact that, as already discussed in Section III, each trajectory i is a realization of the stochastic process—on the target velocity—with a specific set of parameters $\boldsymbol{\theta}_i$. Also the data analysis and the model validation are affected by the inhomogeneity of the samples drawn from different trajectories, these being not directly comparable because of the different process parameters. The validation must, therefore, be carried out by separating the effect of the parameters from the time dependency in the diagonal entries of (12) and in (16)–(19). This is possible by normalizing the error in amplitude for the NCV and in both amplitude and time scale for the OU. Specifically, the error can be normalized as follows

$$\tilde{\boldsymbol{e}}_{\boldsymbol{s}_i}(t) = \begin{cases}\boldsymbol{T}_i^{-1}\boldsymbol{e}_{\boldsymbol{s}_i}(t) & \text{if NCV},\\ \boldsymbol{T}_i^{-1}\boldsymbol{e}_{\boldsymbol{s}_i}(t/\gamma_i) & \text{if OU},\end{cases} \tag{32}$$

where

$$\boldsymbol{T}_i = \begin{cases}\mathrm{diag}\left(\sigma_{x,i}, \quad \sigma_{y,i}, \quad \sigma_{x,i}, \quad \sigma_{y,i}\right) & \text{if NCV},\\ \mathrm{diag}\left(\frac{\sigma_{x,i}}{\gamma_x^{3/2}}, \quad \frac{\sigma_{y,i}}{\gamma_y^{3/2}}, \quad \frac{\sigma_{x,i}}{\gamma_x^{1/2}}, \quad \frac{\sigma_{y,i}}{\gamma_y^{1/2}}\right) & \text{if OU}.\end{cases} \tag{33}$$

In this way the second moment of $\tilde{\boldsymbol{e}}_{\boldsymbol{s}_i}(t)$ is independent of i. Specifically, the error variance can be derived easily from the diagonal elements of (12) and from (16)–(19)

$$\boldsymbol{d}\left(\mathrm{E}\left[\tilde{\boldsymbol{e}}_{\boldsymbol{s}_i}(t)\tilde{\boldsymbol{e}}_{\boldsymbol{s}_i}^T(t)\right]\right) = \boldsymbol{\eta}(t), \tag{34}$$

$$\boldsymbol{\eta}(t) \stackrel{def}{=} \begin{cases} \left[\frac{t^p}{p}, \quad \frac{t^p}{p}, \quad t^{p-2}, \quad t^{p-2}\right]^T & \text{if NCV,} \\ [f(t), \quad f(t), \quad g(t), \quad g(t)]^T & \text{if OU,} \end{cases} \tag{35}$$

where $\boldsymbol{d}(\cdot)$ is the vector of the diagonal elements, $p = 3$ or alternatively $p = 4$ (see discussion in Section II-A); the functions $f(t)$ and $g(t)$ are defined in (20)–(21).

At this point we can verify if the sample covariance of the normalized prediction error, provided by the data, fits the theoretical expectation $\boldsymbol{\eta}(t)$. This is possible by using

$$\boldsymbol{\eta}_K(t) \stackrel{def}{=} \frac{1}{K}\sum_{i=1}^{K} \boldsymbol{d}\left(\tilde{\boldsymbol{e}}_{s_i}(t)\tilde{\boldsymbol{e}}_{s_i}^T(t)\right) \stackrel{K\to\infty}{\to} \boldsymbol{\eta}(t), \tag{36}$$

where the convergence can be intended in mean square or in probability [19]. Roughly speaking, in our case, if K is sufficiently large then the sample variance of the normalized prediction error should be close enough to the expected one $\boldsymbol{\eta}(t)$. In Section V we compare the empirical curve $\boldsymbol{\eta}_K(t)$ with the theoretical curve $\boldsymbol{\eta}(t)$ for both OU and NCV models.

The use of normalized errors (32) implies again the knowledge of the process parameters, which of course are not available, and for this reason we use their estimates in place of the true values.

B. Hypothesis Testing Criterion

A complementary validation method is provided by a test-based criterion. For every trajectory the normalized prediction errors are Gaussian with variance $\boldsymbol{\eta}(t)$. It is therefore possible to build up a test to decide if the error variance is $\boldsymbol{\eta}(t)$, hypothesis $\mathcal{H}_0$, or is larger/smaller, hypothesis $\mathcal{H}_1$. Also we assume that under $\mathcal{H}_1$ the errors are still zero-mean Gaussian distributed. Let us consider observing a set of k normalized prediction errors $\{\tilde{\boldsymbol{e}}_{s_i}(t_n)\}_{n=1}^k$ of the i^{th} trajectory, with $t_n \in [t-\delta, t+\delta]$, $\delta > 0$. If the errors are generated from predictions in nonoverlapped time intervals of the set $\mathcal{T}_i$, then by virtue of (25) these errors are also independent. The decision statistics related to a single element of the error, say the x component[5] $\tilde{e}_{x_i}$ in the time interval centered in t, is based on the log-likelihood ratio (LLR)

$$l_{x,i}(t) = \sum_{n=1}^{k} \log\left(\frac{\mathcal{N}(\tilde{e}_{x_i}(t_n), \eta_x(t_n))}{\mathcal{N}(\tilde{e}_{x_i}(t_n), \bar{\eta}_x(t_n))}\right), \tag{37}$$

where $\eta_x(t_n)$ is the first element of $\boldsymbol{\eta}(t_n)$, $\mathcal{N}(x, \sigma^2)$ is the zero-mean Gaussian function with variance σ^2 evaluated in x, $\bar{\eta}_x(t_n)$ is the variance under the alternative hypothesis $\mathcal{H}_1$. We assume that δ is sufficiently small such that $t_n \approx t$, $\eta_x(t_n) \approx \eta_x(t)$ and $\bar{\eta}_x(t_n) \approx \bar{\eta}_x(t)$. The LLR based test, manipulating (37), is as follows

$$l_{x,i}(t) = \sum_{n=1}^{k} \frac{\tilde{e}_{x_i}^2(t_n)}{\eta_x(t_n)} \begin{cases} \in [\gamma_l, \gamma_u] \text{ decide } \mathcal{H}_0, \\ \text{otherwise decide } \mathcal{H}_1, \end{cases} \tag{38}$$

where if $l_{x,i}(t) < \gamma_l$ then the variance is declared to be lower than the expected one, while if $l_{x,i}(t) > \gamma_u$ then the variance is declared to be higher than the expected one. The test has a convenient nonparametric form in which knowledge of $\bar{\eta}_x(t_n)$ is not required. The thresholds γ_l and γ_u can be computed by imposing the probability of rejection of $\mathcal{H}_0$ under $\mathcal{H}_0$

$$\alpha = 1 - \mathrm{P}\left[l_{x,i}(t) \in [\gamma_l, \gamma_u] \mid \mathcal{H}_0\right].$$

Since $l_{x,i}(t)$ under $\mathcal{H}_0$ is a central χ^2 random variable with k degrees of freedom then we have

$$\alpha = 1 - F_{\chi^2}(\gamma_u, k) + F_{\chi^2}(\gamma_l, k), \tag{39}$$

where $F_{\chi^2}(\cdot, k)$ is the central χ^2 cumulative density function (CDF) with k degrees of freedom. If we allow half chance to declare an increase of variance and half to declare a decrease then the two thresholds are given by

$$\gamma_l = F_{\chi^2}^{-1}(\alpha/2, k), \quad \gamma_u = F_{\chi^2}^{-1}(1-\alpha/2, k). \tag{40}$$

By averaging the decisions of all the trajectories, we compute the empirical acceptance rate of $\mathcal{H}_0$ versus the prediction horizon time:

$$p_{x,K}(t) = \frac{1}{K}\sum_{i=1}^{K} \mathcal{I}\left(l_{x,i}(t) \in [\gamma_l, \gamma_u]\right),$$

where $\mathcal{I}(\cdot)$ is the indicator function. Ideally, if the model is correct and all the parameters are known, the empirical acceptance rate $p_{x,K}(t)$ would converge to the value $1-\alpha$ for $K \to \infty$, where the convergence can be intended in mean square or in probability [19]. In Section V we report the empirical acceptance rate $p_{x,K}(t)$ for both the OU and NCV models versus the prediction horizon time.

V. MODEL VALIDATION USING REAL-WORLD VESSEL TRAFFIC DATA

In this section we provide evidence that the uncertainty of long-term state predictions of nonmaneuvering vessels fits better to the OU—for the velocity—and IOU —for the position—models than what does the NCV model. This evidence is based on the analysis of a significant record of all the maritime traffic in the Mediterranean Sea, collected by STO-CMRE. Specifically, the data set consists of AIS messages broadcast by vessels navigating in the Mediterranean Sea in two months of 2014 and collected by a network of satellite and terrestrial receivers.

Considering that the behavior of a vessel, and especially a nonmaneuvering one, depends greatly on its size and tonnage, the motion characteristics may consequently be significantly different among different vessels. Therefore we subdivide the data set into three categories, each of them being representative of a traffic category: cargo, tanker, and passenger vessels. The ensemble of trajectories, subdivided by traffic category, represents the starting point of our analysis.

An additional step has to be accomplished before the actual analysis can start, because of the models described in Section II being valid under the assumption of a

[5] Note that the same reasoning applies to y and $\dot{x}$,$\dot{y}$.

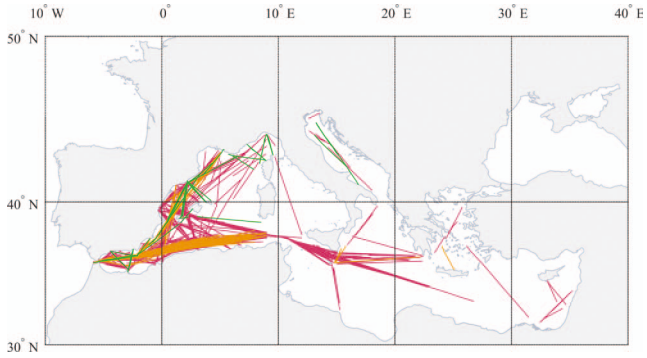

Fig. 4. Quasi-rectilinear trajectories under consideration in the validation study; the color indicates traffic category: pink for the cargo traffic, orange for the tanker, green for the passenger. These trajectories represent a subset of a data set of AIS messages collected over the Mediterranean Sea from multiple AIS networks during two months of 2014.

nonmaneuvering vessel. This preprocessing phase consists of enforcing this assumption on the given real-world data set by breaking every observed trajectory into piecewise "linear" parts where the target has essentially no process noise.[6]

This initial step leaves us with a set of observed trajectories of nonmaneuvering vessels of each traffic category. Fig. 4 illustrates the vessel trajectories that will be used afterwards to perform the analysis of the prediction errors, evaluating the actual prediction error variance against the theoretical models described in Section II.

The prediction procedure is repeated for all the trajectories and for the different motion models, leading us to a collection of prediction errors relative to the target position and velocity as described in Section IV. The OU motion model for the velocity and its integrated version for the position, as described in Section II-A.2, are characterized by three parameters for each coordinate: the noise level $\sigma_{x,y}$, the desired speed $v_{x,y}$, and the reversion rate $\gamma_{x,y}$, which basically represents how quickly the target tends to restore its desired speed after a perturbation. The NCV motion model has instead just one parameter for each coordinate: the noise level $\sigma_{x,y}$.

It is apparent that these process parameters are important to the specific realization but, more importantly, they are not known a priori and therefore have to be estimated, see Section III. The estimation of the process parameters is not error free but, to the contrary, introduces additional error to the prediction error. However, the following analysis shows a good match between the real-data and the theoretical curves, meaning that the trajectory are sufficiently long to guarantee a parameter estimation with a negligible error.

[6] Being on a linear track does not necessarily imply that the vessel is not maneuvering because, especially for long trajectories, it may have changed its velocity quite significantly. However, for the purpose of this work we can safely assume that a vessel under way on a linear track is not a maneuvering target.

A. Single-Target Scenario

In this subsection a single trajectory is analyzed. A tanker vessel of 270 m in length and 48 m in breadth is sailing northeastwards from the Strait of Gibraltar to the East Mediterranean, see Fig. 1. A prediction from the initial point of the trajectory, located in the origin, up to 20 h is performed with both the OU and the NCV models and then compared with the true vessel position. The vessel trajectory is reported in the uppermost part of Fig. 5, along with the OU and NCV predictions and their related uncertainty (95th percentile), as provided by the two models. The covariance matrix is computed assuming that the noise along the direction of the desired velocity is orthogonal to the noise across the same direction as usually assumed, e.g. in [34]. In the lowermost plots of Fig. 5 the vessel velocities along x and y are reported as well as the predicted velocities provided by the models.

This case study shows that even if the NCV prediction is reasonably close to the true vessel position, its uncertainty is disproportionately large. On the other hand, the OU prediction is not only closer to the true vessel position with respect to the NCV prediction but also has a significantly smaller uncertainty (orders of magnitude). The empirical standard deviation (SD) of the prediction errors along x and y with respect to the prediction time horizon is reported in Fig. 6 and compared with the theoretical curves. The empirical SD curves are computed based on the data set related to this single trajectory, see details in Section IV. The empirical curves are more accurate for short-term horizons (< 5 h) because they are computed with more samples with respect to the larger time horizons. For instance, the last point of these curves has just a single sample related to the prediction from the initial point to the last point of the trajectory.

It is worth noticing that the OU and NCV prediction errors are equal in first part (< 1 h) while in the second part they separate and the NCV exhibits a larger error. Furthermore, as already discussed, it is easy to recognize that the NCV model in the very short term (< 10 min) fits sufficiently well the data while in the long term the NCV theoretical curve significantly diverges from the empirical curve. The OU model instead follows the data until 15 h, after this point the empirical curve is not statistically significant because of the lack of samples. In order to have a statistically significant data set we now construct these curves using all the trajectories available as prescribed in Section IV-A.

B. Error Variance Criterion

To keep the notation lighter, let us define a generic coordinate $u = \{x, y\}$ and a generic velocity $\dot{u} = \{\dot{x}, \dot{y}\}$, along its corresponding long-term mean $v = v_{x,y}$, reversion rate $\gamma = \gamma_{x,y}$, and noise term $\sigma = \sigma_{x,y}$. We use subscripts for the time variable, i.e. $u_j = u(t_j)$, when not otherwise stated.

1) *Velocity*: Fig. 7 shows the prediction error variance on the target velocity over the prediction horizon, for the cargo, tanker, and passenger traffic categories. In each

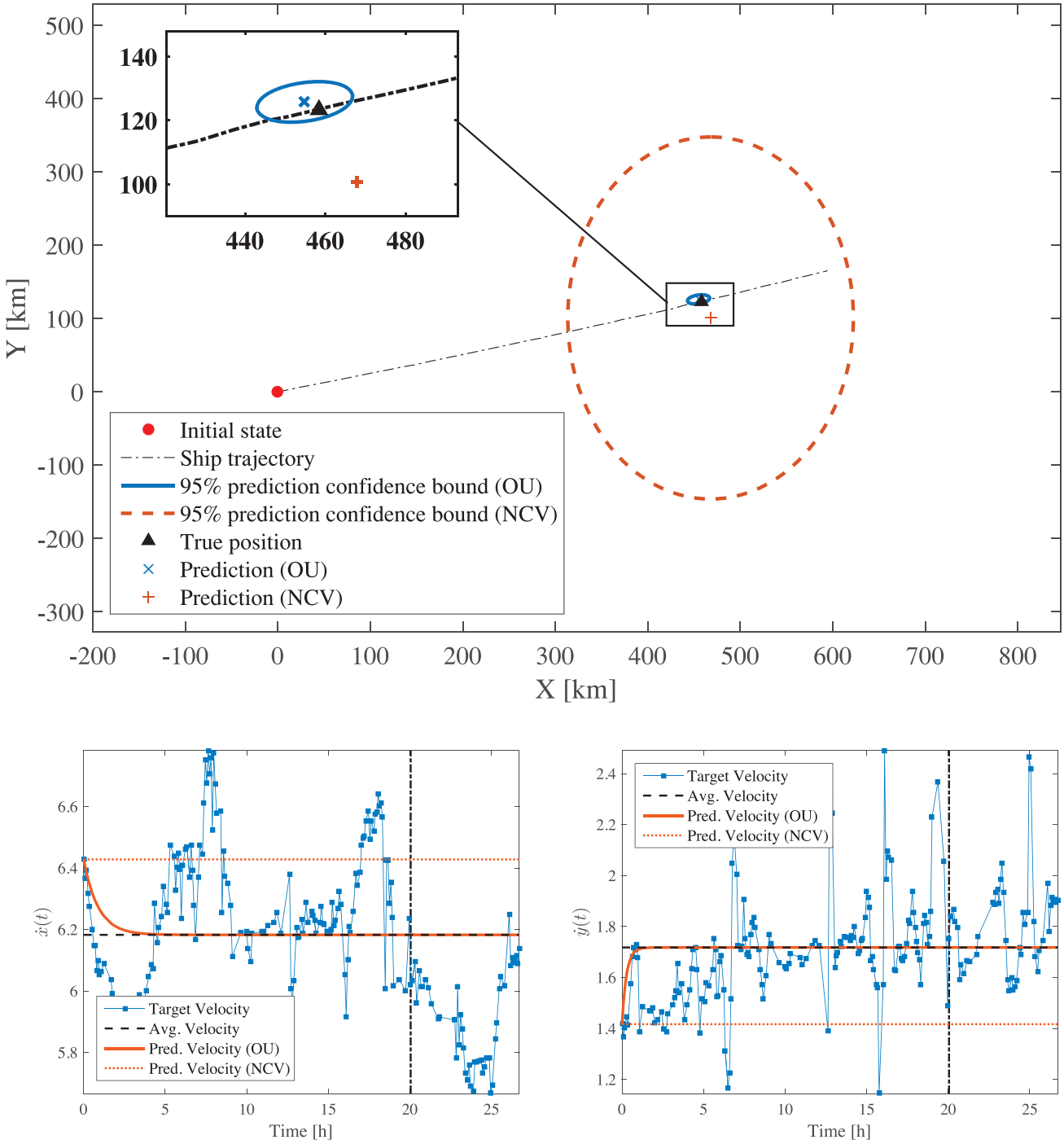

Fig. 5. Single target scenario: comparison of the uncertainty of the predicted positional target state under the assumptions of NCV and OU model. The uppermost illustration reports the highlighted portion of the trajectory in Fig. 1 that has been converted into projected coordinates. The predictions of the target position after approximately 20 hours from the initial state are indicated with cross markers. The related 95%-confidence prediction covariance ellipses are plotted with dashed lines. The two lowermost figures refer to the target velocity along the two components and respectively to the x-coordinate on the left, and the y-coordinate on the right. The actual target velocity samples are drawn with solid lines and square markers. The horizontal black dashed line represents the average observed target velocity in the considered (linear) trajectory segment, while the vertical black dashed line identifies the prediction instant, which happens to be approximatively 20 hours after the initial state. The NCV and OU predictions, given the initial state, are reported in contrast colours with —respectively— dotted and solid lines.

subfigure marker plots illustrate the empirical data, i.e., the actual prediction error variance observed on the target velocity, whereas dashed lines represent the theoretical model.

As discussed in Section IV-A, a normalization step, see (32), is necessary in order to compare the trends of the prediction uncertainty of all the trajectories in the data set. Therefore, the numerical values in OU and NCV plots do

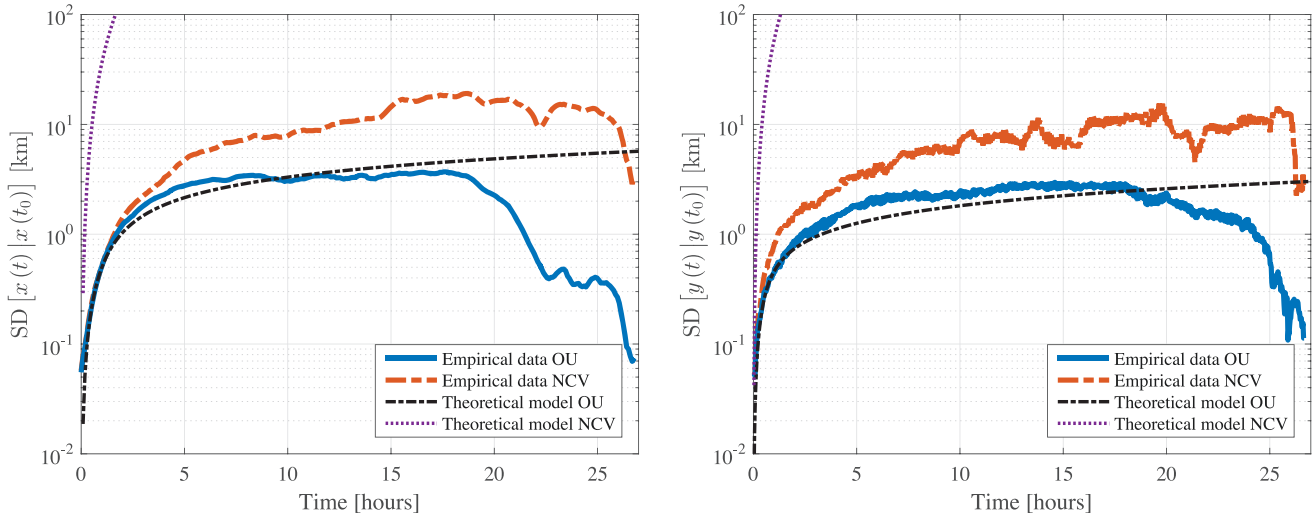

Fig. 6. Single target scenario: unnormalized standard deviation of the prediction error on the target position assuming the OU or NCV motion model, for the two components of the positional target state (x on the left and y on the right). Theoretical curves are reported with dashed lines. The target is given by the tanker vessel whose trajectory is reported in Fig. 1.

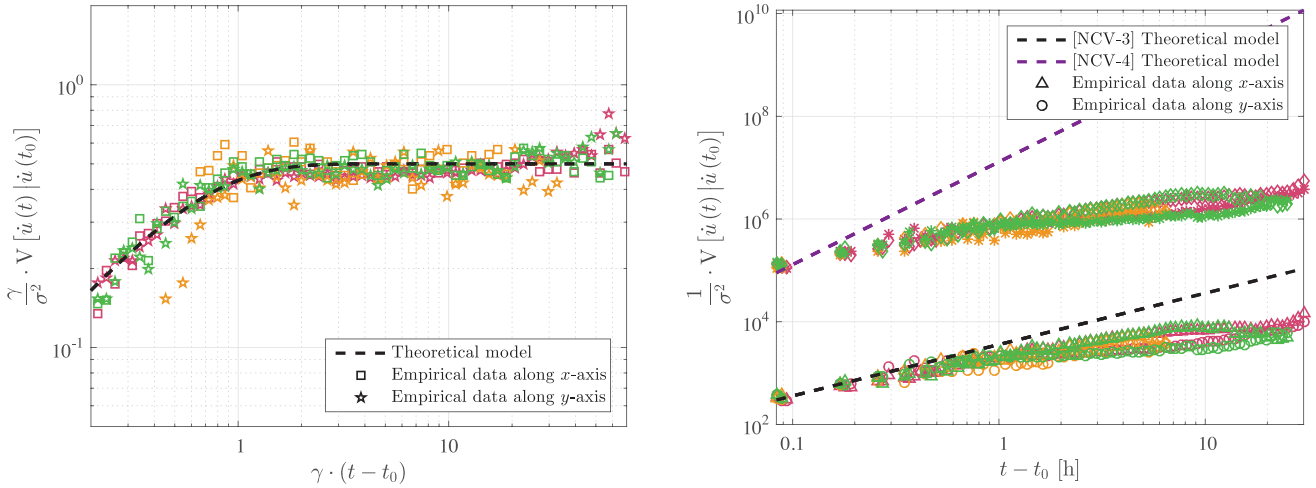

Fig. 7. Normalized variance of the prediction error on target velocity assuming the OU (left) or NCV (right) target motion model, for the three traffic categories: cargo (pink), tanker (green), and passenger (orange). Components along x-axis and y-axis are identified using different markers.

not show the actual variance of the prediction but rather represent the normalized variance function (35). The OU time axis has also been scaled according to the reversion rate of each trajectory. On the contrary, figures with NCV plots need to be scaled only with respect to the noise level, and therefore there is no need to define a normalized time axis. The normalized variance curves are then computed by averaging the error contributes over all the trajectories, see (36).

The aim of these figures is to compare how well the hypothesized models reproduce the evolution of the prediction uncertainty over the prediction horizon. In each of the aforementioned figures, the leftmost graphs are under the OU model hypothesis, while those on the far right relate to the NCV models, in both the cases of $p = 3$ and $p = 4$, see (35).

In Fig. 7 it is easy to recognize that while the NCV models fit the empirical curve only for short time predictions the OU instead fits the whole evolution. It is worth mentioning that in the long term the fundamental difference between the two model becomes clear: the NCV uncertainty diverges, as for a Brownian motion, while the OU reaches an asymptotic level provided by $g(t) \to 1/2$, see (35) and (21). The asymptotic unnormalized OU uncertainty is instead given by $\sigma^2_{x,y}/2\gamma_{x,y}$, basically it is proportional to the noise variance $\sigma^2_{x,y}$ and to the inverse of the reversion rate $1/\gamma_{x,y}$. As already explained in Section II, the NCV model is equivalent to the OU for $\gamma_{x,y} \to 0$, this explains from another point of view why the NCV uncertainty diverges.

2) *Position*: Fig. 8 illustrates how the prediction error variance on the target position varies over the prediction horizon for the cargo, tanker, and passenger traffic categories. As before, marker plots have been used for the empirical data and dashed lines for the theoretical models.

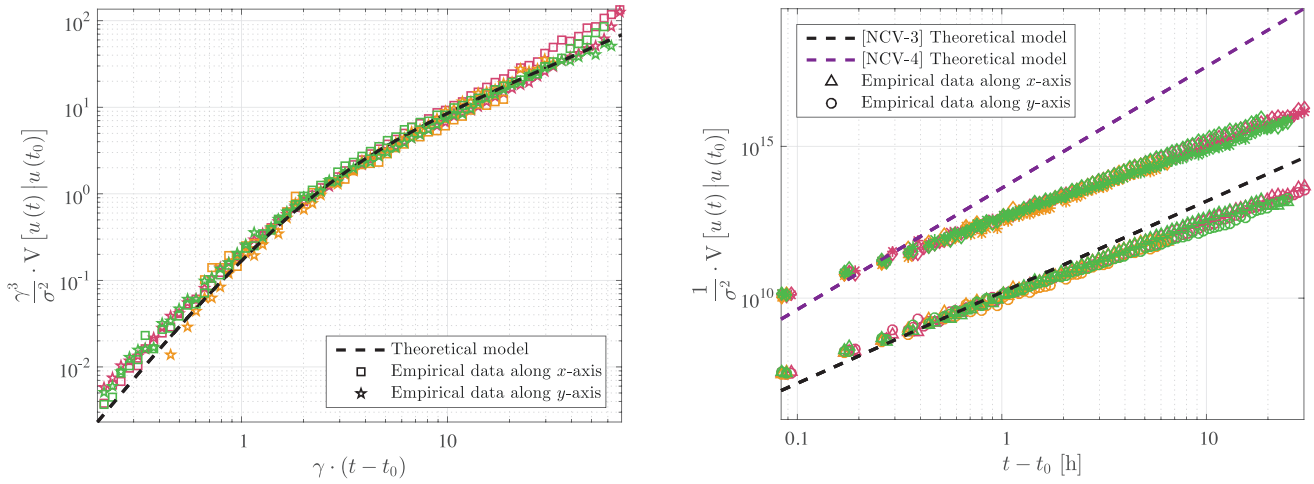

Fig. 8. Normalized variance of the prediction error on the target position assuming the OU (left) or NCV (right) target motion model, for the three traffic categories: cargo (pink), tanker (green), and passenger (orange). Components along x-axis and y-axis are identified using different markers.

Like the OU model for the target velocity, the IOU is apparently more appropriate to model the uncertainty growth over the prediction horizon, especially for long-term target state prediction, where the actual prediction error variance on the position of the target is several orders of magnitude below the value one would expect according to both versions of the NCV.

As opposed to the velocity curve, the position uncertainty diverges for both IOU and NCV, see (35) and (20). However, the divergence rates are different, specifically the normalized IOU uncertainty grows as t while the NCV grows as t^p with $p = 3$ or $p = 4$. The growth rate for the unnormalized IOU uncertainty is ruled by σ^2/γ^3, as opposed to the asymptotic variance of the velocity, this being proportional to the cube of the reversion rate.

C. Hypothesis Testing Criterion

In this section we report the empirical results of the hypothesis testing validation criteria discussed in Section IV-B. Specifically, in Fig. 9 it is reported the $\mathcal{H}_0$ decision rate for the OU and NCV models. Based on the assumptions made in Section IV-B, we test whether the empirical errors are statistically compatible with the theoretical model $\mathcal{H}_0$, which states that the normalized squared errors are distributed as a central χ^2 distribution with a variance provided by (35). Under the alternative hypothesis $\mathcal{H}_1$ the errors are still χ^2 distributed but with a variance different from (35). The test, under the aforementioned assumptions, is nonparametric in the sense that one needs to know only the parameters under $\mathcal{H}_0$ but not under $\mathcal{H}_1$. However, the parameters under $\mathcal{H}_0$ are unknown and can only be estimated; this means that the normalized errors, using estimated parameters, are approximately χ^2 distributed. Because of this approximation we can have a higher rejection rate of $\mathcal{H}_0$ with respect to the prescribed α.

The rate of decision in favor of $\mathcal{H}_0$ is computed by averaging the decisions made for each individual trajectory at every time interval. The confidence level adopted was $\alpha = 5\%$.

The unsuitability of the NCV models for long-term prediction is evident here, but as already discussed, in the short term the NCV model is equally suitable, from a statistical point of view, to the OU model. On the contrary, as already observed in the previous subsection, the OU model is statistically compatible with the empirical errors and the acceptance rate in favor of the hypothesized model is constantly close to $1 - \alpha = 95\%$ for all the prediction time horizon.

D. Statistics of OU Parameters

As already mentioned, each trajectory in the data set is characterized by a different set of parameters $\boldsymbol{\theta} = (\boldsymbol{\theta}_x, \boldsymbol{\theta}_y)$ of the underlying OU process. The procedure described in Appendix B leaves us with an estimate, in the ML sense, of the parameters γ, σ, and v. Fig. 10 shows how these parameters are distributed for the three different categories of maritime traffic. Each plot in the figure shows the joint distribution of γ and σ along the two coordinates of the reference system rotated along the direction of motion, defined by $\boldsymbol{v}$. In other words, in the rotated plane $(x_\perp, y_\parallel)$ the characteristic speed across the trajectory is always null, i.e. $v_{x_\perp} = 0$. For completeness sake, in Table I we report some statistics that have been computed on the same data set, i.e. mean, median, and SD values.

It can be seen that, for all the traffic categories, the across-track reversion rate is higher than the along-track one, in terms of both average (mean and median values) and variability (standard deviation), and it is reflected also in Figs. 10(a)–10(c), where the peaks of the estimated joint distribution all fall below the bisection line of the first quadrant. Practically, vessels adjust their across-track velocity faster than the along-track one. This is also in line with what one would expect considering that

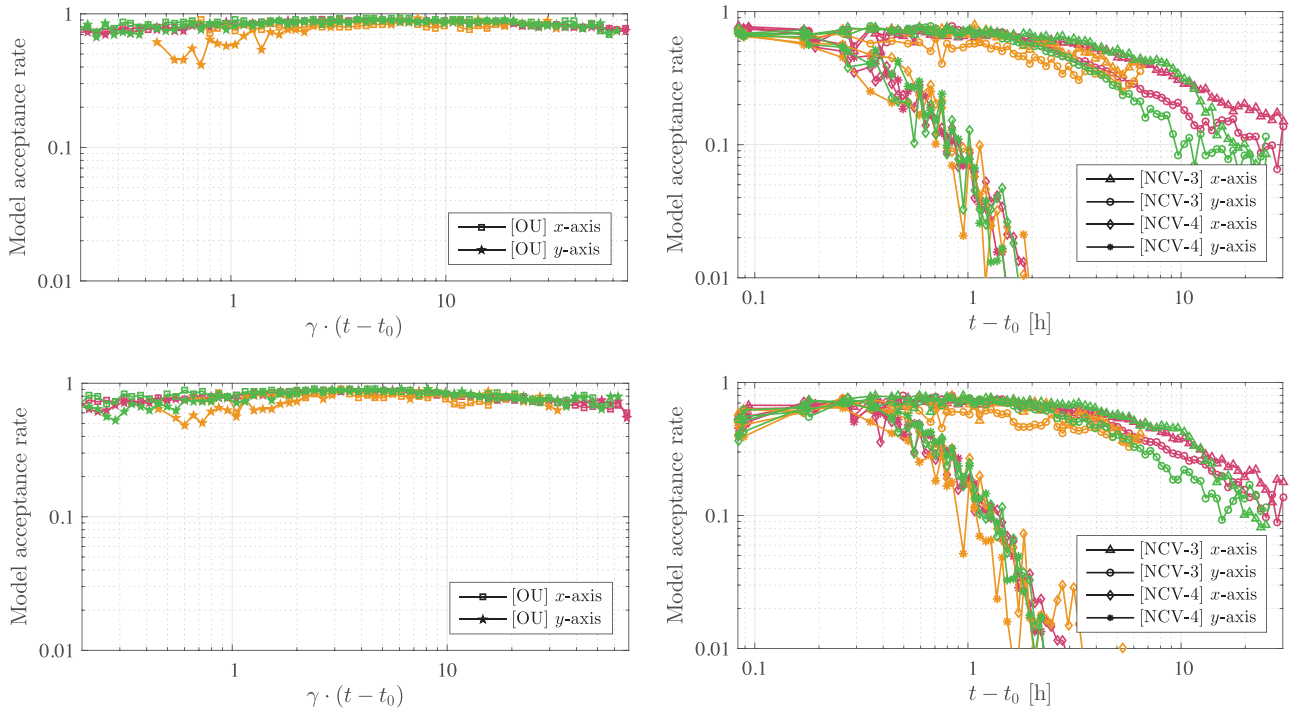

Fig. 9. Model acceptance rate of OU (left) and NCV (right) target motion model as function of the prediction time based on the velocity (top) and position (bottom) error components, for the three traffic categories: cargo (pink), tanker (green), and passenger (orange). Nominal rejection rate $\alpha = 5\%$. Different markers are used for x and y components.

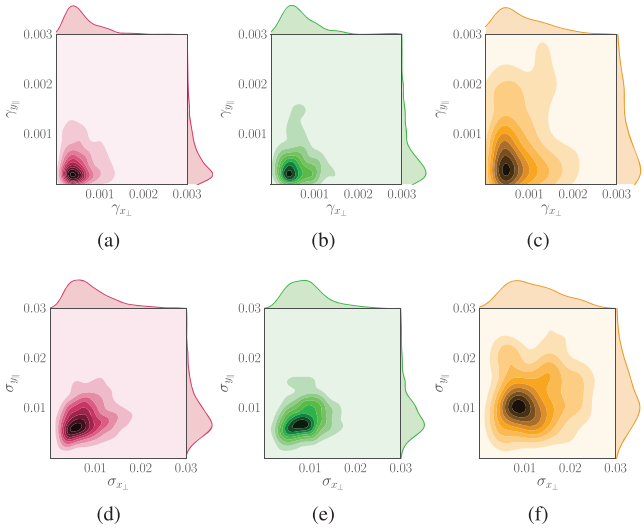

Fig. 10. Joint distributions of OU process parameter estimates for the three traffic categories: cargo (a) and (d), tanker (b) and (e), and passenger (c) and (f). Univariate graphs (i.e. empirical marginal distributions) are shown on two axes. Figures (a)–(c) refer to reversion rate γ, while (d)–(f) at the bottom show joint distribution of process noise σ. The x-axis and y-axis refer, respectively, to across-track and along-track coordinate.

TABLE I
Statistical Features of OU Process Estimated Parameters for Three Traffic Categories

			γ	σ
Cargo	Mean	$y_\parallel$	5.63×10^{-4}	9.17×10^{-3}
		$x_\perp$	6.28×10^{-4}	9.04×10^{-3}
	Median	$y_\parallel$	3.79×10^{-4}	7.95×10^{-3}
		$x_\perp$	5.11×10^{-4}	7.90×10^{-3}
	SD	$y_\parallel$	5.41×10^{-4}	4.92×10^{-3}
		$x_\perp$	4.41×10^{-4}	5.00×10^{-3}
Tanker	Mean	$y_\parallel$	5.40×10^{-4}	8.89×10^{-3}
		$x_\perp$	7.31×10^{-4}	9.47×10^{-3}
	Median	$y_\parallel$	3.81×10^{-4}	7.80×10^{-3}
		$x_\perp$	6.02×10^{-4}	8.95×10^{-3}
	SD	$y_\parallel$	4.98×10^{-4}	4.39×10^{-3}
		$x_\perp$	5.11×10^{-4}	4.49×10^{-3}
Passenger	Mean	$y_\parallel$	8.18×10^{-4}	1.26×10^{-2}
		$x_\perp$	8.36×10^{-4}	1.20×10^{-2}
	Median	$y_\parallel$	5.68×10^{-4}	1.11×10^{-2}
		$x_\perp$	7.13×10^{-4}	1.11×10^{-2}
	SD	$y_\parallel$	7.54×10^{-4}	5.83×10^{-3}
		$x_\perp$	5.63×10^{-4}	5.59×10^{-3}

physically—under the nonmaneuverability hypothesis—the tonnage of a vessel does not simply allow sudden significant changes of the along-track velocity, while significant variations to the across-track one can be easily implemented via the rudder. The process noise parameter distributions, reported in Figs. 10(d)–10(f), are approximately symmetric with the peaks of the estimated joint distribution falling along the bisection line of the first quadrant.

It is worth mentioning that the OU process is well suited for the representation of the long-term state prediction uncertainty also in the rotated plane. Roughly speaking, the procedures described in Sections IV-A and IV-B could be repeated on the rotated coordinates, leading to a situation similar to what is shown in Figs. 7–9.

The assumption of a diagonal reversion rate matrix is adopted also in the rotated plane, even if this matrix cannot possibly be diagonal both in the original and rotated planes. However, the data analysis suggests that the effect of the cross-reversion terms is negligible. On the other hand, from a theoretical perspective, the most general problem of a coupled OU process is addressed and the corresponding solution is provided in Appendix A.

$$\boldsymbol{\Sigma}_2(t) = \begin{bmatrix} f(t\gamma_x) & h(t,\boldsymbol{\gamma}) & k(t\gamma_x) & \frac{g(\gamma_y \frac{t}{2})}{\gamma_y} - \frac{g((\gamma_x+\gamma_y)\frac{t}{2})}{\gamma_x+\gamma_y} \\ h(t,\boldsymbol{\gamma}) & f(t\gamma_y) & \frac{g(\gamma_x \frac{t}{2})}{\gamma_x} - \frac{g((\gamma_x+\gamma_y)\frac{t}{2})}{\gamma_x+\gamma_y} & k(t\gamma_y) \\ k(t\gamma_x) & \frac{g(\gamma_x \frac{t}{2})}{\gamma_x} - \frac{g((\gamma_x+\gamma_y)\frac{t}{2})}{\gamma_x+\gamma_y} & g(t\gamma_x) & g((\gamma_x+\gamma_y)\frac{t}{2}) \\ \frac{g(\gamma_y \frac{t}{2})}{\gamma_y} - \frac{g((\gamma_x+\gamma_y)\frac{t}{2})}{\gamma_x+\gamma_y} & k(t\gamma_y) & g((\gamma_x+\gamma_y)\frac{t}{2}) & g(t\gamma_y) \end{bmatrix} \tag{41}$$

VI. CONCLUSION

In this paper the problem of issuing long-term predictions of future target states has been studied, with specific focus on the modeling of the related uncertainty. That is, given a target motion model, the aim has been to derive an optimal prediction procedure and investigate its variance over the prediction horizon. However, unlike most of the literature in the tracking field, our efforts have concentrated on the case of long-term target state prediction, where the prediction horizon is orders of magnitude above the refresh rate of the sensor issuing the observation, being this case much more plausible in the real-world problem of maritime traffic motion modeling.

Two different stochastic motion models have been hypothesized, the first being the well-known NCV model, and the second less commonly studied—at least in the tracking literature— OU mean-reverting stochastic model. A detailed description and comparison of the two theoretical models has been provided and it is accompanied by an extensive validation study on a real-world data set which is representative of a significant portion of the maritime traffic in the Mediterranean Sea. Experimental results confirm that OU stochastic processes may be used to model the motion of nonmaneuvering vessels while under way. Its major advantage over the more traditional NCV model is that the variance of the predicted position grows linearly with the prediction horizon, resulting in a prediction uncertainty that is much more contained in larger time scales.

In the future, this model may be applied to relevant scenarios that might benefit from a more accurate modeling of the prediction uncertainty. For example, in the task of satellite image acquisition, the reduction of uncertainty in vessel location could enable higher resolution imagery over a smaller area, thus providing more accurate classification. Future investigations are needed to study on-line procedures for estimating and updating the OU parameters while the data are observed.

APPENDIX A. COUPLED OU PROCESS

Let us consider the SDE (8); as already mentioned, the solution can be found using Itô calculus [15, 24] and the first two moments are as follows

$$\boldsymbol{s}(t|t_0) = \mathrm{e}^{\boldsymbol{A}(t-t_0)}\boldsymbol{s}(t_0) + \int_{t_0}^{t} \mathrm{e}^{\boldsymbol{A}(t-s)}\boldsymbol{G}\boldsymbol{v}\mathrm{d}s, \tag{42}$$

and

$$\mathrm{Cov}\left[\boldsymbol{s}(t)\,|\boldsymbol{s}(t_0)\right] = \int_{t_0}^{t} \mathrm{e}^{\boldsymbol{A}(t-s)}\boldsymbol{B}\boldsymbol{B}^T\left(\mathrm{e}^{\boldsymbol{A}(t-s)}\right)^T \mathrm{d}s. \tag{43}$$

We define $\boldsymbol{\Gamma} = \mathrm{diag}\,(\boldsymbol{\gamma})$, $\boldsymbol{\gamma}$ being the vector of eigenvalues of $\boldsymbol{\Theta}$. Assuming that $\boldsymbol{\Theta}$ diagonalizable, $\boldsymbol{\Theta} = \boldsymbol{R}\boldsymbol{\Gamma}\boldsymbol{R}^{-1}$ represents its eigendecomposition, and the following relations hold

$$\boldsymbol{A} = \begin{bmatrix} \boldsymbol{0} & \boldsymbol{I} \\ \boldsymbol{0} & -\boldsymbol{\Theta} \end{bmatrix} = \begin{bmatrix} \boldsymbol{0} & \boldsymbol{I} \\ \boldsymbol{0} & -\boldsymbol{R}\boldsymbol{\Gamma}\boldsymbol{R}^{-1} \end{bmatrix} = \widetilde{\boldsymbol{R}}\widetilde{\boldsymbol{A}}\widetilde{\boldsymbol{R}}^{-1},$$

where

$$\widetilde{\boldsymbol{R}} \overset{def}{=} \begin{bmatrix} \boldsymbol{R} & \boldsymbol{0} \\ \boldsymbol{0} & \boldsymbol{R} \end{bmatrix} \quad \text{and} \quad \widetilde{\boldsymbol{A}} \overset{def}{=} \begin{bmatrix} \boldsymbol{0} & \boldsymbol{I} \\ \boldsymbol{0} & -\boldsymbol{\Gamma} \end{bmatrix}. \tag{44}$$

We can now exploit the power series of the matrix exponential to obtain a convenient expression for $\mathrm{e}^{\boldsymbol{A}t}$

$$\begin{aligned} \mathrm{e}^{\boldsymbol{A}t} &= \sum_{k=0}^{\infty} \frac{1}{k!}\boldsymbol{A}^k t^k \\ &= \sum_{k=0}^{\infty} \frac{1}{k!} \prod_{i=0}^{k} \left(\widetilde{\boldsymbol{R}}\,\widetilde{\boldsymbol{A}}\widetilde{\boldsymbol{R}}^{-1}\right) t^k \\ &= \sum_{k=0}^{\infty} \frac{1}{k!}\,\widetilde{\boldsymbol{R}}\,\widetilde{\boldsymbol{A}}^k t^k \widetilde{\boldsymbol{R}}^{-1} \\ &= \widetilde{\boldsymbol{R}} \left(\sum_{k=0}^{\infty} \frac{1}{k!}\,\widetilde{\boldsymbol{A}}^k t^k\right) \widetilde{\boldsymbol{R}}^{-1} \\ &= \widetilde{\boldsymbol{R}}\mathrm{e}^{\widetilde{\boldsymbol{A}}t}\,\widetilde{\boldsymbol{R}}^{-1}, \end{aligned} \tag{45}$$

that can be reworked to highlight the dependence on t and $\boldsymbol{\gamma}$

$$\boldsymbol{\Phi}(t,\boldsymbol{\gamma}) \stackrel{def}{=} \mathrm{e}^{\widetilde{\boldsymbol{A}}t} = \begin{bmatrix} \boldsymbol{I} & \left(\boldsymbol{I} - \mathrm{e}^{-\boldsymbol{\Gamma} t}\right)\boldsymbol{\Gamma}^{-1} \\ \boldsymbol{0} & \mathrm{e}^{-\boldsymbol{\Gamma} t} \end{bmatrix}. \tag{46}$$

On the other hand, the integral in (42) can be written in terms of $\boldsymbol{\Phi}(t,\boldsymbol{\gamma})$

$$\begin{aligned} \boldsymbol{\Psi}(t,\boldsymbol{\gamma}) &\stackrel{def}{=} \int_{t_0}^{t} \mathrm{e}^{\boldsymbol{A}(t-s)}\,\boldsymbol{G}\,\mathrm{d}s \\ &= \int_{t_0}^{t} \boldsymbol{\Phi}(t-s,\boldsymbol{\gamma}) \begin{bmatrix} \boldsymbol{0} \\ \boldsymbol{\Gamma} \end{bmatrix} \mathrm{d}s, \end{aligned} \tag{47}$$

and allows a closed-form solution

$$\boldsymbol{\Psi}(t,\boldsymbol{\gamma}) = \begin{bmatrix} t\,\boldsymbol{I} - \left(\boldsymbol{I} - \mathrm{e}^{-\boldsymbol{\Gamma} t}\right)\boldsymbol{\Gamma}^{-1} \\ \boldsymbol{I} - \mathrm{e}^{-\boldsymbol{\Gamma} t} \end{bmatrix}. \tag{48}$$

Combining together (42), (46), and (48) leads us to the first moment of the SDE solution, which has the form

$$\begin{aligned} \boldsymbol{s}(t\,|t_0) = {} & \widetilde{\boldsymbol{R}}\boldsymbol{\Phi}(t-t_0,\boldsymbol{\gamma})\,\widetilde{\boldsymbol{R}}^{-1}\boldsymbol{s}(t_0) \\ & + \widetilde{\boldsymbol{R}}\boldsymbol{\Psi}(t-t_0,\boldsymbol{\gamma})\,\widetilde{\boldsymbol{R}}^{-1}\boldsymbol{v}, \end{aligned} \tag{49}$$

where $\boldsymbol{\Phi}(t,\boldsymbol{\gamma})$ is the state transition matrix and $\boldsymbol{\Psi}(t,\boldsymbol{\gamma})$ is the control input function, defined as before.

We can proceed analogously with the second-order solution using (43) and (46)

$$\begin{aligned} &\mathrm{Cov}\left[\boldsymbol{s}(t)\,|\boldsymbol{s}(t_0)\right] \\ &= \widetilde{\boldsymbol{R}} \left(\int_{t_0}^{t} \boldsymbol{\Phi}(t-s,\boldsymbol{\gamma}) \begin{bmatrix} \boldsymbol{0} & \boldsymbol{0} \\ \boldsymbol{0} & \widetilde{\boldsymbol{C}} \end{bmatrix} \boldsymbol{\Phi}^{T}(t-s,\boldsymbol{\gamma})\,\mathrm{d}s \right) \widetilde{\boldsymbol{R}}^{-1} \end{aligned} \tag{50}$$

where $\widetilde{\boldsymbol{C}}$ is the noise covariance in the transformed domain, whose entries are defined as follows

$$\widetilde{\boldsymbol{C}} \stackrel{def}{=} \boldsymbol{R}^{-1}\boldsymbol{C}\left(\boldsymbol{R}^{-1}\boldsymbol{C}\right)^{T} = \begin{bmatrix} \sigma_x^2 & \sigma_{xy} \\ \sigma_{xy} & \sigma_y^2 \end{bmatrix}.$$

Again, the problem can be solved in algebraically closed form and for the second moment of the SDE solution, we obtain

$$\mathrm{Cov}\left[\boldsymbol{s}(t)\,|\boldsymbol{s}(t_0)\right] = \widetilde{\boldsymbol{R}}\,\boldsymbol{\Sigma}(t-t_0)\,\widetilde{\boldsymbol{R}}^{-1}, \tag{51}$$

where $\boldsymbol{\Sigma}(t) = \boldsymbol{\Sigma}_1 \circ \boldsymbol{\Sigma}_2(t)$. The matrix $\boldsymbol{\Sigma}_1$ has the following form

$$\boldsymbol{\Sigma}_1 = \begin{bmatrix} \dfrac{\sigma_x^2}{\gamma_x^3} & \dfrac{\sigma_{xy}}{\gamma_x\gamma_y} & \dfrac{\sigma_x^2}{2\gamma_x^2} & \dfrac{2\sigma_{xy}}{\gamma_x} \\ \dfrac{\sigma_{xy}}{\gamma_x\gamma_y} & \dfrac{\sigma_y^2}{\gamma_y^3} & \dfrac{2\sigma_{xy}}{\gamma_y} & \dfrac{\sigma_y^2}{2\gamma_y^2} \\ \dfrac{\sigma_x^2}{2\gamma_x^2} & \dfrac{2\sigma_{xy}}{\gamma_y} & \dfrac{\sigma_x^2}{\gamma_x} & \dfrac{2\sigma_{xy}}{\gamma_x+\gamma_y} \\ \dfrac{2\sigma_{xy}}{\gamma_x} & \dfrac{\sigma_y^2}{2\gamma_y^2} & \dfrac{2\sigma_{xy}}{\gamma_x+\gamma_y} & \dfrac{\sigma_y^2}{\gamma_y} \end{bmatrix} \tag{52}$$

and $\boldsymbol{\Sigma}_2(t)$ is defined in (41). This latter equation is finally completed by the following function definitions of $f(t)$, $g(t)$—that have already been defined in (20) and (21)—$h(t,\gamma)$ and $k(t)$

$$\begin{aligned} f(t) &\stackrel{def}{=} \frac{1}{2}\left(2t + 4\mathrm{e}^{-t} - \mathrm{e}^{-2t} - 3\right) \\ g(t) &\stackrel{def}{=} \frac{1}{2}\left(1 - \mathrm{e}^{-2t}\right) \\ h(t,\boldsymbol{\gamma}) &\stackrel{def}{=} t - \frac{1-\mathrm{e}^{-t\gamma_x}}{\gamma_x} - \frac{1-\mathrm{e}^{-t\gamma_y}}{\gamma_y} \\ &\quad + \frac{1-\mathrm{e}^{-t(\gamma_x+\gamma_y)}}{\gamma_x+\gamma_y}, \end{aligned} \tag{54}$$

$$k(t) \stackrel{def}{=} \mathrm{e}^{-2t}\left(1-\mathrm{e}^{t}\right)^2. \tag{55}$$

APPENDIX B. PROCESS PARAMETER ESTIMATION

As previously noted, let us define a generic coordinate $u = \{x, y\}$ and a generic velocity $\dot{u} = \{\dot{x}, \dot{y}\}$, along with its corresponding long-term mean $v = v_{x,y}$, reversion rate $\gamma = \gamma_{x,y}$, and noise term $\sigma = \sigma_{x,y}$. Also when not otherwise stated, the subscripts are used to indicate the time variable, i.e., $u_j = u(t_j)$, for $j = 1, \ldots, n$, n being the number of observed target states within a given rectilinear trajectory.

A. NCV Model Process Parameter Estimation

The NCV likelihood can be derived from (26) or (27) specialized by (28a)–(28d), obtaining

$$\mathcal{L}(\boldsymbol{\theta}) = \mathcal{L}(\sigma) = \prod_{j=1}^{n} \frac{1}{\sqrt{2\pi}\sigma}\, e^{-\frac{\left(\dot{u}_j - \dot{u}_{j-1}\right)^2}{2\sigma^2\Delta_j}} \tag{56}$$

Omitting the constant term, the log-likelihood has the form

$$\ell(\sigma) = -n\log\sigma - \frac{1}{2\sigma^2}\sum_{j=1}^{n} \frac{\left(\dot{u}_j - \dot{u}_{j-1}\right)^2}{\Delta_j}. \tag{57}$$

The ML estimate is provided by the most likely parameter

$$\hat{\sigma} = \max_{\sigma} \ell(\sigma).$$

The maximum condition is the following

$$\frac{\partial\ell(\sigma)}{\partial\sigma} = -\frac{n}{\sigma} + \frac{1}{\sigma^3}\sum_{j=1}^{n} \frac{\left(\dot{u}_j - \dot{u}_{j-1}\right)^2}{\Delta_j} = 0, \tag{58}$$

which leads to

$$\hat{\sigma} = \sqrt{\frac{1}{n}\sum_{j=1}^{n} \frac{\left(\dot{u}_j - \dot{u}_{j-1}\right)^2}{\Delta_j}}. \tag{59}$$

B. OU Model Process Parameter Estimation

The OU process defined by (8) can be stationary, Gaussian, and Markovian and it is an example of a Gaussian process with bounded variance and stationary probability distribution, as opposed to the Wiener process.

This is due to the fact that in the latter the drift term is constant, whereas in the OU it is dependent on the current value of the process: if it is less than the long-term mean, the drift will be positive; on the contrary, if the current value is higher than the long-term mean, the drift will be negative. This behavior gives the name mean-reverting.

In this appendix we provide a description of the ML procedure used for the estimation of process parameters given a set of observations, see further details in [14]. Let us consider a single vessel trajectory, representing a realization of the OU process. We observe a set of velocities on the generic coordinate observed along a single quasi-rectilinear vessel trajectory. Let this set be

$$\mathcal{Z} = \{\dot{u}_i\}_{j=0}^{n}.$$

In Section III the generic form of the likelihood of the observation, given the observations $\mathcal{Z}$, has been already provided in (25) as well as its specialization for the two Cartesian components of the target velocity (26) and (27).

Under the assumptions of stationarity, Gaussianity, and Markovianity of the OU process, the log-likelihood of $\mathcal{Z}$ can be derived from (26) or (27) specialized by (29a)–(29d). Omitting the constant terms, the log-likelihood has the form

$$\ell(\boldsymbol{\theta}) = -\frac{n}{2}\log\left(\frac{\sigma^2}{2\gamma}\right) - \frac{1}{2}\sum_{j=1}^{n}\log\left[1-\mathrm{e}^{-2\gamma\Delta_j}\right] - \frac{\gamma}{\sigma^2}\sum_{j=1}^{n}\frac{\left(\dot{u}_j - v - \left(\dot{u}_{j-1}-v\right)\mathrm{e}^{-\gamma\Delta_j}\right)^2}{1-\mathrm{e}^{-2\gamma\Delta_j}} \quad (60)$$

where n is the cardinality of the time intervals in $\mathcal{Z}$ and $\boldsymbol{\theta} = (v, \gamma, \sigma)$ is the set of process parameters. The term $\Delta_j = t_j - t_{j-1}$ represents the time elapsed between the j-th and the immediately previous observation, enabling eventually the possibility of estimating also the parameters of asynchronous OU processes ($\Delta_j \neq \Delta_k, j \neq k$).

The ML estimate $\hat{\boldsymbol{\theta}} = (\hat{v}, \hat{\gamma}, \hat{\sigma})$ given $\mathcal{Z}$ is the one that satisfies the following first-order conditions

$$\left.\frac{\partial\ell(\boldsymbol{\theta})}{\partial v}\right|_{\hat{v}} = 0, \quad \left.\frac{\partial\ell(\boldsymbol{\theta})}{\partial\gamma}\right|_{\hat{\gamma}} = 0, \quad \left.\frac{\partial\ell(\boldsymbol{\theta})}{\partial\sigma}\right|_{\hat{\sigma}} = 0. \quad (61)$$

The log-likelihood (60) can be elaborated and leads us to the marginal likelihood of $\mathcal{Z}$ with respect to v

$$\frac{\partial\ell(\boldsymbol{\theta})}{\partial v} = -\frac{\gamma}{\sigma^2}\sum_{j=1}^{n}\frac{\dot{u}_j - v - \left(\dot{u}_{j-1}-v\right)\mathrm{e}^{-\gamma\Delta_j}}{1+\mathrm{e}^{-\gamma\Delta_j}}. \quad (62)$$

Assuming γ and σ are nonzero, the first order conditions (61) lead us to the ML estimate of the long-term mean of the process:

$$\hat{v} = f(\hat{\gamma}) = \sum_{j=1}^{n}\frac{\dot{u}_j - \dot{u}_{j-1}\mathrm{e}^{-\hat{\gamma}\Delta_j}}{1+\mathrm{e}^{-\hat{\gamma}\Delta_j}}\left(\sum_{j=1}^{n}\frac{1-\mathrm{e}^{\hat{\gamma}\Delta_j}}{1+\mathrm{e}^{\hat{\gamma}\Delta_j}}\right)^{-1}. \quad (63)$$

From here, following the same approach as before, we can differentiate (60) with respect to σ, thus obtaining the marginal log-likelihood of $\mathcal{Z}$

$$\frac{\partial\ell(\boldsymbol{\theta})}{\partial\sigma} = -\frac{n}{\sigma} + \frac{2\gamma}{\sigma^3}\sum_{j=1}^{n}\frac{\left(\dot{u}_j - v - \left(\dot{u}_{j-1}-v\right)\mathrm{e}^{-\gamma\Delta_j}\right)^2}{1-\mathrm{e}^{-2\gamma\Delta_j}}, \quad (64)$$

which, if combined with conditions (61), provides an estimate of the noise term σ

$$\hat{\sigma} = g(\hat{v}, \hat{\gamma}) = \sqrt{\frac{2\hat{\gamma}}{n}\sum_{j=1}^{n}\frac{\left(\dot{u}_j - \hat{v} - \left(\dot{u}_{j-1}-\hat{v}\right)\mathrm{e}^{-\hat{\gamma}\Delta_j}\right)^2}{1-\mathrm{e}^{-2\hat{\gamma}\Delta_j}}}.$$

The system of nonlinear equations given by $\hat{v} = f(\hat{\gamma})$ and $\hat{\sigma} = g(\hat{v}, \hat{\gamma})$ together with conditions (61) would lead to the ML estimator, but the solution would not be available in closed form. A different approach is to substitute $\hat{v} = f(\hat{\gamma})$ and $\hat{\sigma} = g(\hat{v}, \hat{\gamma})$ directly into the likelihood function (60), obtaining the following

$$V(\gamma) = -\frac{n}{2}\log\left(\frac{g(f(\gamma)), \gamma)^2}{2\gamma}\right) - \frac{1}{2}\sum_{j=1}^{n}\log\left(1-\mathrm{e}^{-2\gamma\Delta_j}\right) - \frac{\gamma}{\tilde{g}_\gamma^2}\sum_{j=1}^{n}\frac{\left(\dot{u}_j - f(\gamma) - \left(\dot{u}_j - f(\gamma)\right)\mathrm{e}^{-\gamma\Delta_j}\right)^2}{1-\mathrm{e}^{-2\gamma\Delta_j}}, \quad (65)$$

having defined $\tilde{g}_\gamma = g(f(\gamma), \gamma)$. Contrary to the solution of the aforementioned system of nonlinear equations, the minimization of (65) is a one-dimensional search problem, whose solution can be shown to be the ML estimator of γ

$$\hat{\gamma} = \arg\min_{\gamma} V(\gamma).$$

ACKNOWLEDGMENT

L. M. Millefiori, P. Braca, and K. Bryan wish to thank the NATO Allied Command Transformation (ACT) for supporting the project Data Knowledge Operational Effectiveness (DKOE) at the NATO Science and Technology Organization (STO) Centre for Maritime Research and Experimentation (CMRE).

The authors gratefully acknowledge the initial contributions to the formulation of this study by Steven Horn and Giuliana Pallotta.

REFERENCES

[1] IMO. International Maritime Organization Safety of Life at Sea (SOLAS) Convention. Chapter V, Regulation 19, 2014.

[2] NATO. Alliance Maritime Strategy, official texts, Mar. 2011.

[3] Bar-Shalom, Y., Willett, P., and Tian, X. *Tracking and Data Fusion: A Handbook of Algorithms.* Storrs, CT: YBS Publishing, Apr. 2011.

[4] Barndorff-Nielsen, O. E., and Shephard, N. Integrated OU processes and non-Gaussian OU-based stochastic volatility models. *Scandinavian Journal of Statistics*, **30**, 2 (June 2003), 277–295.

[5] Blackwell, P.
Random diffusion models for animal movement.
Ecological Modelling, **100**, 1 (1997), 87–102.

[6] Braca, P., Willett, P., LePage, K., Marano, S., and Matta, V.
Bayesian tracking in underwater wireless sensor networks with port-starboard ambiguity.
IEEE Transactions on Signal Processing, **62**, 7 (2014), 1864–1878.

[7] Capraro, G., Farina, A., Griffiths, H., and Wicks, M.
Knowledge-based radar signal and data processing: A tutorial review.
IEEE Signal Processing Magazine, **23**, 1 (Jan. 2006), 18–29.

[8] Christensen, H. L., Murphy, J., and Godsill, S. J.
Forecasting high-frequency futures returns using online Langevin dynamics.
IEEE Journal of Selected Topics in Signal Processing, **6**, 4 (Aug. 2012), 366–380.

[9] Coraluppi, S., and Carthel, C.
A hierarchical MHT approach to ESM-radar fusion.
In *2012 15th International Conference on Information Fusion (FUSION)*, July 2012, 677–683.

[10] Coraluppi, S., and Carthel, C.
Stability and stationarity in target kinematic modeling.
In *IEEE Aerospace Conference*, Mar. 2012, 1–8.

[11] Coraluppi, S., and Carthel, C.
Advances in multi-target filtering of evasive targets.
In *2015 IEEE Aerospace Conference*, Mar. 2015, 1–8.

[12] Coraluppi, S., and Carthel, C.
Stochastic data association in multi-target filtering.
In *Proceedings of SPIE*, Vol. **8393**, 2012, 83 930Q–83 930Q–7.

[13] Einstein, A.
On the movement of small particles suspended in stationary liquids required by the molecular-kinetic theory of heat.
Annalen der Physik, **17** (1905), 549–560.

[14] Franco, J. C. G.
Maximum likelihood estimation of mean reverting processes.
Real Options Practice (2003).

[15] C. W. Gardiner, C. W. et al. *Handbook of Stochastic Methods*, Vol. **4**. Berlin: Springer, 1985.

[16] Gillespie, D.
Exact numerical simulation of the Ornstein-Uhlenbeck process and its integral.
Physical Review E, **54**, 2 (1996), 2084–2091.

[17] Grasso, R., Braca, P., Osler, J., Hansen, J., and Willett, P.
Optimal asset network planning for counter piracy operation support, part 1: Under the hood.
IEEE Aerospace and Electronic Systems Magazine, **29**, 5 (May 2014), 4–11.

[18] Langevin, P.
Sur la théorie du mouvement Brownien.
Comptes Rendus de l'Académie des Sciences (1908), 530–533.

[19] Lehmann, E.
Elements of Large Sample Theory. New York: Springer, 2004.

[20] Li, X. R., and Jilkov, V.
Survey of maneuvering target tracking. Part II. Motion models of ballistic and space targets.
IEEE Transactions on Aerospace and Electronic Systems, **46**, 1 (Jan. 2010), 96–119.

[21] Maresca, S., Braca, P., Horstmann, J., and Grasso, R.
Maritime surveillance using multiple high-frequency surface-wave radars.
IEEE Transactions on Geoscience and Remote Sensing, **52**, 8 (Aug. 2014), 5056–5071.

[22] Millefiori, L. M., Pallotta, G., Horn, S., Braca, P., and Bryan, K.
Validation of the Ornstein-Uhlenbeck route propagation model in the Mediterranean Sea.
In *Proceedings of the OCEANS'15 MTS/IEEE Conference*, May 2015, 1–7.

[23] International Telecommunication Union, Radio Communication Sector (ITU-R).
Technical characteristics for an automatic identification system using time-division multiple access in the VHF maritime mobile band, Recommendation ITU-R M.1371-5, (Feb. 2014), 1–148.

[24] Øksendal, B.
Stochastic Differential Equations. New York: Springer, 2003.

[25] Pallotta, G., Horn, S., Braca, P., and Bryan, K.
Context-enhanced vessel prediction based on Ornstein-Uhlenbeck processes using historical AIS traffic patterns: Real-world experimental results.
In *2014 17th International Conference on Information Fusion (FUSION)*, July 2014, 1–7.

[26] Pallotta, G., Vespe, M., and Bryan, K.
Vessel pattern knowledge discovery from AIS data: A framework for anomaly detection and route prediction.
Entropy, **15**, 6 (2013).

[27] Ristic, B., La Scala, B., Morelande, M., and Gordon, N.
Statistical analysis of motion patterns in AIS data: Anomaly detection and motion prediction.
In *Proceedings of the 11th International Confeence on Information Fusion (FUSION)*, Florence, Italy, 2008.

[28] Li, X. R., and Jilkov, V.
Survey of maneuvering target tracking. Part I. Dynamic models.
IEEE Transactions on Aerospace and Electronic Systems, **39**, 4 (Oct. 2003), 1333–1364.

[29] Stone, L. D., Barlow, C. A., and Corwin, T. L.
Bayesian Multiple Target Tracking. Norwood, MA: Artech House, 1999.

[30] Tuckwell, H., Wan, F., and Rospars, J.-P.
A spatial stochastic neuronal model with Ornstein–Uhlenbeck input current.
Biological Cybernetics, **86**, 2 (2002), 137–145.

[31] Uhlenbeck, G. E., and Ornstein, L. S.
On the theory of Brownian motion.
Physical Review, **36** (1930), 823–841.

[32] Valdivieso, L., Schoutens, W., and Tuerlinckx, F.
Maximum likelihood estimation in processes of Ornstein-Uhlenbeck type.
Statistical Inference for Stochastic Processes, **12**, 1 (2009), 1–19.

[33] Vespe, M., Visentini, I., Bryan, K., and Braca, P.
Unsupervised learning of maritime traffic patterns for anomaly detection.
In *9th IET Data Fusion Target Tracking Conference (DFTT 2012): Algorithms Applications*, May 2012.

[34] Vivone, G., Braca, P., and Horstmann, J.
Knowledge-based multi-target tracking via UKF-JPDA variable structure IMM estimator in HF surface wave radar systems.
IEEE Transactions on Geoscience and Remote Sensing (2015).

[35] Wang, H., Kirubarajan, T., and Bar-Shalom, Y.
Precision large scale air traffic surveillance using IMM/assignment estimators.
IEEE Transactions on Aerospace and Electronic Systems, **35**, 1 (Jan. 1999), 255–266.

[36] Benavoli, A., Chisci, L., Farina, A., Timmoneri, L. and Zappa, G.
Knowledge-based system for multi-target-tracking in a littoral environment, *IEEE Transactions on Aerospace and Electronic Systems*, **42**, 3 (July 2006), 1100–1119.

Leonardo M. Millefiori (S'12–M'14) was born in Scorrano, LE, Italy, on October 22, 1988. He attended the Sapienza University of Rome, Italy, where he received his B.Sc. degree in Aerospace Information Engineering in and his M.Sc. degree summa cum laude in Communication Engineering with focus on radar systems and remote sensing, in September 2010 and January 2013, respectively. From June to December 2013, he was Visiting Researcher at the NATO Science & Technology Organization Centre for Maritime Research and Experimentation (CMRE), that he joined in 2014 as Scientist under the Maritime Security Programme. His current research interests include target motion modeling, statistical signal processing, target tracking and data fusion and radar systems.

Paolo Braca received the Laurea degree (summa cum laude) in electronic engineering, and the Ph.D. degree (highest rank) in information engineering from the University of Salerno, Italy, in 2006 and 2010, respectively. In 2009, he was a Visiting Scholar with the Department of Electrical and Computer Engineering, University of Connecticut, Storrs, CT, USA. In 20102011, he was a Postdoctoral Associate with the University of Salerno, Italy. In 2011, he joined the NATO Science & Technology Organization Centre for Maritime Research and experimentation (CMRE) as a Scientist with the Research Department. Dr. Braca conducts research in the general area of statistical signal processing with emphasis on detection and estimation theory, wireless sensor network, multiagent algorithms, target tracking and data fusion, adaptation and learning over graphs, distributed radar (sonar) processing.

Karna Bryan attended Yale University (M.A. Statistics, 1996) and the University of Nebraska-Lincoln (B.S. with Highest Distinction in Mathematics, 1994). She is currently Programme Manager of the Maritime Security Programme at the NATO Center for Maritime Research and Experimentation. Her current research interests are to focus interdisciplinary research to applied research challenges in the area of maritime data fusion and anomaly detection. Her specific interest are to progress scalable approaches to multi-sensor, multi-source fusion problems, including the treatment information variety, quality and uncertainty. She began her career as an operations research scientist working in risk assessment and developing measures of performance and effectiveness for specific user communities.

Peter Willett (F'03) received his B.A.Sc. (engineering science) from the University of Toronto in 1982, and his Ph.D. degree from Princeton University in 1986. He has been a faculty member at the University of Connecticut ever since, and since 1998 has been a Professor. His primary areas of research have been statistical signal processing, detection, machine learning, data fusion and tracking. He also has interests in and has published in the areas of change/abnormality detection, optical pattern recognition, communications and industrial/security condition monitoring. He is editor-in-chief of IEEE Signal Processing Letters. He was editor-in-chief for IEEE Transactions on Aerospace and Electronic Systems (2006-2011), and was Vice President for Publications for AESS (2012-2014).

Document Data Sheet

Security Classification		Project No.
Document Serial No.	**Date of Issue**	**Total Pages**
CMRE-PR-2019-088	June 2019	18 pp.

Author(s)

Leonardo M. Millefiori, Paolo Braca, Karna Bryan, Peter Willett

Title

Modeling vessel kinematics using a stochastic mean-reverting process for long-term prediction

Abstract

We present a novel method for predicting long-term target states based on mean-reverting stochastic processes. We use the Ornstein-Uhlenbeck (OU) process, leading to a revised target state equation and to a time scaling law for the related uncertainty that in the long term is shown to be orders of magnitude lower than under the nearly constant velocity (NCV) assumption. In support of the proposed model, an analysis of a significant portion of real-world maritime traffic is provided.

Keywords

Mathematical model, predictive models, trajectory, uncertainty, stochastic processes, target tracking

Issuing Organization

NATO Science and Technology Organization
Centre for Maritime Research and Experimentation

Viale San Bartolomeo 400, 19126 La Spezia, Italy

[From N. America:
STO CMRE
Unit 31318, Box 19, APO AE 09613-1318]

Tel: +39 0187 527 361
Fax:+39 0187 527 700

E-mail: library@cmre.nato.int